Journal of Photochemistry and Photobiology 10 (2022) 100121

Contents lists available at ScienceDirect

Journal of Photochemistry and Photobiology

journal homepage: www.sciencedirect.com/journal/journal-of-photochemistry-and-photobiology

Nanobiophotonics. Effect of carbon nanoparticles on the optical and spectroscopic properties of *Cichorium intybus* leaves

Rocio Torres [a,b], Virginia Emilse Diz [b], María Gabriela Lagorio [a,b,*]

[a] CONICET, Universidad de Buenos Aires, INQUIMAE, Facultad de Ciencias Exactas y Naturales, Buenos Aires, Argentina
[b] Universidad de Buenos Aires, Facultad de Ciencias Exactas y Naturales, Dpto. de Química Inorgánica, Analítica y Química Física, Ciudad Universitaria, Pabellón II, 1er piso, Buenos Aires, C1428EHA Argentina

ARTICLE INFO

Keywords:
Carbon nanoparticles
Chlorophyll-a fluorescence
Photosynthesis
Nanoparticles toxicity
Reflectance indexes
OJIP transient

ABSTRACT

The effect of different types of nanoparticles on plants has been of great interest in recent years. Within this general context, the specific purpose of the present work was to study the interaction between carbon nanoparticles and the photosynthetic electron chain, to determine whether they induced a beneficial or toxic effect on the primary steps of photosynthesis. Two types of nanoparticles were synthesized and physicochemically characterized: nanocarbon black (nano-CB) and graphene quantum dots (GQD). They were sprayed over *Cichorium intybus* leaves and their effect on the photosynthetic chain was studied using chlorophyll-a fluorescence analysis. Nano-CB was prepared by an acid exfoliation method from commercial carbon black, whereas GQD were obtained by pyrolysis of L-glutamic acid. The nanoparticulate systems displayed luminescent properties and the fluorescence quantum yield for GQD resulted about six times higher than the value for nano-CB. Both kind of nanoparticles presented similar effects on the plant leaves, but the action of GQD was more pronounced. They induced an evident decrease in the content of photosynthetic pigments, a reduced xanthophyll cycle and a lower ability to dissipate excess energy by non-photochemical quenching. Changes in the concentration ratios Chlorophyll a/b and Chlorophylls/Carotenoids were similar to those previously found for shaded leaves but could not be assigned to shading effects in this case. The results of this work suggested a particular deleterious action on the performance of photosystem I (PSI). The phytotoxicity of the tested carbon nanoparticles on *Cichorium intybus,* at the level of the primary photosynthesis stages was, thus, demonstrated.

1. Introduction

In recent times, the topic concerning the adequate use of energy in the world has gained increasing prominence. In this context, photosynthesis represents an essential process in relation to the use of solar energy for carbon assimilation and biomass production, with relevance at a global level [1]. Improving the photosynthetic process is evidently a matter of interest and nanoparticles (Nps) are involved in new methodologies developed for this purpose. In fact, the use of nanotechnology in plant growth has increased lately due to the novel properties of nanoparticulate materials that allow their use in different applications such as nutrition [2], pathogen control [3] or controlled delivery of chemicals [4], among others. In the last decade, many studies dealing with the interaction between nanoparticles and photosynthetic material were published, showing both detrimental and beneficial effects [5,6]. Nanoparticles are also relevant to the development of sensors and imaging technologies with applications in environmental sensing [7]. Therefore, research on the consequences of the interaction of nanoparticles with plants is essential, either for crop production or for environmental protection.

In particular, carbon-based nanomaterials have been considered the most discussed and used nanomaterials over the last decade. Carbon nanoparticles or carbon dots (CDs) have been classified as a remarkable type of recently developed quasi-spherical carbonaceous nanomaterials, their sizes smaller than 10 nm [8,9]. Although it has not been long since the discovery of CDs in 2004, carbon quantum dots have been the subject of numerous optical research studies to be used in areas such as biomonitoring, sensing, photocatalysis, drug and gene delivery, solar conversion and LED technology [10]. Thanks to the existence of numerous carboxylic moieties on their surface, CDs have excellent water solubility and may be chemically functionalized. Furthermore, CDs have been used in light energy conversion applications [11,12], since they are

* Corresponding author.
E-mail address: mgl@qi.fcen.uba.ar (M.G. Lagorio).

https://doi.org/10.1016/j.jpap.2022.100121

Available online 25 April 2022
2666-4690/© 2022 The Author(s). Published by Elsevier B.V. This is an open access article under the CC BY-NC-ND license (http://creativecommons.org/licenses/by-nc-nd/4.0/).

good electron donors and acceptors [13,14]. Other unique properties of CDs, including a well-defined shape; small dimensions; harmonic and adjustable surface functionalities; and their simple, fast, inexpensive, and non-toxic synthesis procedures, make them a promising alternative to other nanoparticles,

CDs mainly include GQDs (graphene quantum dots), CNDs (carbon nanodots), and PDs (polymers dots). GQDs have one or more layers of graphene and functional groups (carboxylic, hydroxyl, amino, etc., depending on the synthesis route) connected at their edges. CNDs are always spherical and classified into two categories: carbon nanoparticles, which do not have a crystal lattice, and carbon quantum dots (CQDs), which have an obvious crystal lattice. Due to the diversity of CDs, different approaches can be adopted for their preparation, the most common ones being "top-down" cutting from different carbon sources (often forming GQD or CND), and "bottom-up" synthesis (from organic molecules or polymers and the modification of the functionality of the surface) [15,16]. Carbon dots have become a rising star in carbon-based nanomaterials thanks to their fluorescent properties, high chemical stability, tolerance to photobleaching, good functionalization capacity and low biological toxicity. It is for these reasons that they are chosen as fluorescent labels for biological and chemical analysis, and for fluorescence imaging [17].

Research work on the interactions of carbonaceous nanomaterials (fullerenes, nanotubes, QDs, nano-onions, nano-horns, among others) with plants has been reported [8,18–21]. Nanoparticles can penetrate plants either via their leaves or via their roots. Two routes for solute absorption through the cuticle exist, one accessible for non-polar solutes through diffusion and permeation (lipophilic pathway) and another one for polar solutes, which enter through aqueous pores (hydrophilic pathway) with an estimated effective size ranging from 0.6 to 4.8 nm [22]. Consequently, Nps with diameters below 4.8 nm can penetrate directly through the cuticular pathway. Additionally, many studies have reported foliar uptake and accumulation of Nps larger than 5 nm, although the pathway by which these Nps are absorbed is still unclear. Moreover, in addition to the cuticular pathway, some studies have demonstrated the uptake of hydrophilic substances through stomatal apertures. The morphological size of stomatal apertures is approximately 25 μm in length and 3 to 10 μm in width [22]. Numerous studies support this uptake pathway by the observation of several Nps or their aggregates in leaf stomata and deeper tissues of different plant species, using electron microscopy and X-ray micrographs, among others [23,24].

Once nanoparticles were taken by plants through an aerial or root pathway, beneficial or adverse effect on plant growth and productivity could be observed. The results were dependent on the composition, concentration, size, and coating of nanoparticles.

Milenković *et al.* recently found that low concentration (≈ 1mg/L) of CDs, foliarly applied on Maize, increased the photosynthesis rate measured by the uptake of CO_2 [25]. Enhanced photosynthesis was also observed by Chandra *et al.* [26]. They detected electron transfer from carbon dots to chloroplasts of mung bean plants and they found that oxygen evolution, non-cyclic photophosphorylation and ATP synthesis were improved in the presence of these nanoparticles. Despite the above-mentioned promoting functions of CDs on the growth of various crop plants, inhibition of crop development was also observed [9]. As an example, after the exposure of maize seeds to high concentrations of CDs (2000 mg/L), the fresh weights of the roots and shoots of the resulting plants were significantly reduced and oxidative damage was identified [27].

A large number of research studies on the interaction between nanoparticles and plants have been conducted, but most of them are mainly based on measurements of plant and root growth, leaf development, oxidative stress and variations in pigment content. Works that focus on the effect of nanoparticles on the early stages of photosynthesis, on the partitioning of the absorbed energy and on the consequences over the electronic transport chain are not frequent. Considering this vacancy in literature, the specific purpose of the present work was to study the interaction between carbon nanoparticles and the photosynthetic electron chain, to determine whether they induced a beneficial or toxic effect on the primary steps of photosynthesis.

In this research, and based on the previously published bibliography, two types of carbon nanoparticles, GQDs and CNDs, were prepared in order to study their interaction with plant material. Two alternative working hypotheses were formulated here:

i The prepared carbon nanoparticles will interfere in the processes of energy and electron transfer within chloroplasts and will have a deleterious effect on photosynthesis.
ii The prepared carbon nanoparticles will enhance energy absorption by plants and will benefit the photosynthetic process.

These two hypotheses were analyzed by means of a series of spectroscopic techniques (mainly reflectance and chlorophyll-fluorescence) that allow inferring damage or improvement at the photosynthetic chain level.

2. Materials and methods

2.1. Nanoparticle synthesis

Two types of carbon nanoparticles were prepared by a top-down and by a bottom-up method. They were respectively named Nano-carbon black (nano-CB) and graphene quantum dots (GQD). Nano-CB was prepared by an acid exfoliation method from commercial carbon black (Full Black S.R.L., average diameter of 10-300 nm). The procedure was based on previously reported techniques [28–30]. In brief, carbon black (1 g) was dispersed in water and sonicated for 30 minutes, to deagglomerate its solid particles and improve their wetting. Then, 50 mL of a mixture of 30% H_2O_2 and H_2SO_4(c), in a ratio of approximately 3:1, was added. The mixture was refluxed at 80°C for 3 hours and allowed to cool. Once it has reached room temperature, acetone was added, to obtain a solution with 10% by volume of acetone and centrifuged at 20,000 RPM for 15 minutes. The acid-containing supernatant remaining from the reaction was discarded, and the precipitate was dispersed in water and neutralized with NaOH (s) to neutral pH. During this process, Na_2SO_4 precipitated and was cold filtered, in order to reduce the concentration of this salt in the resulting nanoparticle dispersion. Finally, the sample was centrifuged again adding a small quantity of acetone to facilitate nanoparticles precipitation [31]. The precipitation and redispersion processes were repeated several times until their impurities were sufficiently removed. The precipitate was suspended in distilled water and stored for subsequent spectroscopic characterization.

On the other hand, GQD were synthesized following Wu *et al.* (2013) [32]. Briefly, 2.0 g of L-glutamic acid was added into an appropriate beaker and heated at 210°C. During heating, the solid L-glutamic melted and turned brown in about 45 seconds. Then, 15 ml of water was added while stirring for 10 min. The solution was cooled to room temperature and centrifuged at 22,000 RPM during 30 min. Finally, the supernatant, containing GQD, was collected and stored for further characterization.

2.2. Nanoparticle characterization

UV-VIS absorption spectra were recorded using a double-beam spectrophotometer (UV-3600 Plus, Shimadzu, Tokyo, Japan). Excitation-emission matrices and fluorescence quantum yields of the nanoparticles were obtained with a steady-state spectrofluorometer (QuantaMaster, PTI-Photon Technology International-Brunswick, USA), using a 90° geometry. Determinations of fluorescence quantum yields were performed as described elsewhere [33]. A solution of Rhodamine 101 in ethanol was used as fluorescence reference and measurements were carried out in triplicates. Both absorption and fluorescence measurements were performed on nanoparticles suspensions.

IR spectra of the synthesized solid nanomaterials were recorded with a Nicolet 8700 FTIR spectrophotometer with a resolution of 4 cm^{-1} using an ATR accessory.

The morphology of the nanoparticles was observed under a Zeiss SUPRA 40 scanning electron microscope (SEM) operated at 20 kV, and a Phillips EM 301 transmission electron microscope, operated at 60 kV; both with a resolution of 5 nm. Microscopy samples were prepared by drop-casting: drops of dilute dispersions of nanoparticles were deposited on appropriate grids and allowed to dry.

All the determinations were carried out at room temperature.

2.3. Plant growth and nanoparticle application

Fourteen chicory (*Cichorium intybus*) seedlings were acquired from a plant nursery and acclimatized for 30-45 days under LED irradiation[1] (photosynthetic photon flux density (PPFD) 300 μmol m^{-2} s^{-1}), 16-hour photoperiod) and controlled irrigation, at an average temperature of 25°C. Nano-CB and GQD dispersions in distilled water (absorbance value at maximum = 0.2) were applied on these plant leaves using a sprayer. The resulting concentrations were at 1.15 g/L (≈ 9 10^{18} Np/mL) for GQD and 2.3 g/L (≈ 2 10^{19} Np/mL) for nano-CB. The application was performed on four plants for each treatment (a total of twelve plants were employed: four plants were used as control, four were treated with nano-CB and four treated with GQD) and a volume of 25 mL of each suspension was sprayed on the leaves, at each application. For the control samples, distilled water, instead of nanoparticle dispersions, was sprayed on the leaves. Fully developed leaves were sprayed once a day, twice a week for a total period of four weeks. Afterwards, detection and analysis of optical and spectroscopic parameters were carried out for control and treated plants.

2.4. Pigment content of plant leaves

Leaves were cut from each plant (control and treated samples), washed with distilled water and the central veins and petioles were removed. A mortar was used to extract pigments with 80% (V/V) acetone, which were then centrifuged for 3 to 5 minutes at 3000 RPM. A suitable dilution of the resulting extract was immediately assayed by UV-VIS spectrophotometry (UV-3600 Plus, Shimadzu, Tokyo, Japan) and the contents of Chlorophyll-a (Chl a), Chlorophyll-b (Chl b) and carotenoids (Cars) were determined according to Lichtenthaler and Buschmann (2005) [34].

Pigment content was reported in μg cm^{-2} of leaf area. Weight ratios Chl a/b and Chls/Cars were also calculated. Twelve plants were used: four controls, four plants treated with nano-CB and four plants treated with GQD. From each group of four plants, 8 leaves were collected, by detaching two leaves from each plant. Pigment extraction and quantification were carried out on these 8 leaves. The determination was repeated for each treatment on another group of 8 leaves collected in the same way.

2.5. Diffuse reflectance and spectral indexes of plant leaves

Diffuse reflectance spectra (R(λ)) as a function of wavelength (λ) were determined for optically thick layers composed of several leaves (4-5 leaves), so that the transmittance was null in the entire visible region. For this purpose, a spectrophotometer (3101PC, Shimadzu, Tokyo, Japan) equipped with an integrating sphere was employed. Barium sulfate was used to adjust 100% reflectance. Zero transmittance for the thick layer of leaves was a condition for the application of the correction model to account for light re-absorption processes in steady state fluorescence spectra.

From reflectance values, several spectral indexes were calculated: the normalized difference vegetation index, NDVI (Eq. (1), [35]), the modified normalized difference vegetation index, mNDVI (Eq. (2), [35]), the photochemical reflectance index, PRI (Eq. (3), [35]), the Pigment Specific Normalized Difference for Chlorophyll a, PSNDa (Eq. (4), [36]) and the Pigment Specific Normalized Difference for Chlorophyll b, PSNDb (Eq. (5), [36]).

$$NDVI = \frac{R_{800\ nm} - R_{680\ nm}}{R_{800\ nm} + R_{680\ nm}} \quad (1)$$

$$mNDVI = \frac{R_{750\ nm} - R_{705\ nm}}{R_{750\ nm} + R_{705\ nm} - 2\,R_{445\ nm}} \quad (2)$$

$$PRI = \frac{R_{531\ nm} - R_{570\ nm}}{R_{531\ nm} + R_{570\ nm}} \quad (3)$$

$$PSND_a = \frac{R_{800\ nm} - R_{675\ nm}}{R_{800\ nm} + R_{675\ nm}} \quad (4)$$

$$PSND_b = \frac{R_{800\ nm} - R_{650\ nm}}{R_{800\ nm} + R_{650\ nm}} \quad (5)$$

2.6. Plant leaves. Variable chlorophyll fluorescence. Kautsky's Kinetics

Variable chlorophyll fluorescence was recorded *in vivo*, using a pulse-amplitude-modulated chlorophyll fluorometer (FMS1, Hansatech Instruments Ltd., UK) on non-detached leaves, previously dark-adapted for 15 min as described elsewhere [37]. The experimental protocol is outlined in Fig. 1.

Measurements were started by recording the minimum fluorescence signal of the dark- adapted samples (F_0), with only the modulation beam on for 30 seconds. This beam had very short duration pulses (1.8 μs), with long off period between pulses, and the integrated number of photons incident upon the leaves was very small (PPFD < 0.05 μmol $m^{-2}s^{-1}$).Then, a saturation pulse (PPFD = 2700 μmol m^{-2} s^{-1}) was applied to determine the maximum fluorescence (F_M). After stabilization of the fluorescence for 30 seconds, an actinic light (AL) of PPFD = 12 μmol m^{-2} s^{-1} was turned on for a total of 7 minutes. A saturating pulse was then applied to record F_M'. The protocol was repeated for higher AL: PPFD = 185 μmol m^{-2} s^{-1} and 627 μmol m^{-2} s^{-1}.

The procedure was replicated on five different leaves of each plant for each treatment. From the analysis of variable fluorescence, the following photosynthetic parameters were obtained: the initial fluorescence of dark adapted leaves, F_0; the maximum fluorescence for dark-adapted leaves, F_M; the variable fluorescence for dark-adapted leaves, F_v (F_M - F_0); the ratio between variable and maximum fluorescence, F_v/F_M [2]; the ratio between variable and initial fluorescence, F_v/F_0; the maximum chlorophyll fluorescence for light-adapted leaves, F_M'; the stationary fluorescence for light-adapted leaves, Fs; the quantum yield of photophysical decay, Φc (F_s/F_M); the quantum yield of non-photochemical quenching, Φ_{NPQ} ($Fs.(F_M-F_M')/(F_M.F_M')$); the efficiency of PSII, Φ_{PSII} ($F_M'-F_S/F_M'$); the photosynthetic rate of PSII, PS_{rate} (Φ_{PSII}. AL, with Al: intensity of the actinic light); the coefficient for the photochemical quenching, qP, ($(F_M'-F_s)/(F_M'-F_0)$) and the coefficient for

[1] A combination of 6 cool white light lamps (Philips, EcoHome LEDBulb 14W E27 6500KHV, 910 lm/W; technical sheet at: https://bit.ly/35BtfVC) and 6 warm light lamps (Philips, EcoHome LEDBulb 12W E27 3000KHV, 910 lm/W; technical sheet at: https://bit.ly/3pKI92C) was used.

[2] The ratio F_v/F_M has been historically considered as the maximum quantum yield of photosynthesis for dark-adapted leaves. However, recent research highlights that this ratio cannot be strictly considered equivalent to the photochemical efficiency of PSII [85]. These authors demonstrated that F_v, which has been traditionally assigned to the transition from the open to the close states of PSII reaction center, has an important transition contribution from the closed state to a light-adapted charge separated state of PSII. This last transition was shown to be associated to light-induced conformational variations in the core complexes.

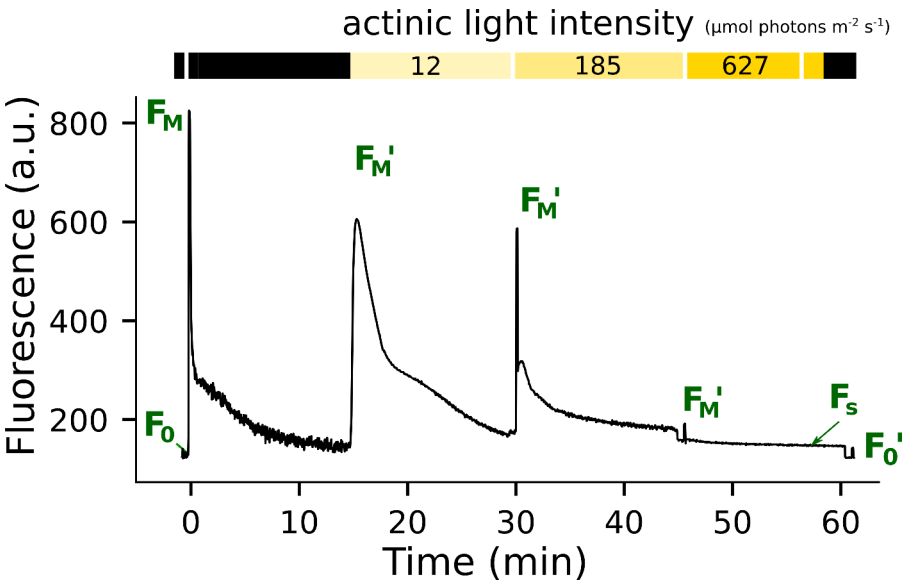

Fig. 1. Kautsky's kinetics. Scheme of the measuring protocol. The upper bar shows the intensity of the actinic light as a function of the intensity of the yellow color. The black portions represent the dark phase where the actinic light is off. F0 is the initial fluorescence signal of the dark- adapted leaves, FM is the maximum fluorescence after applying a light saturation pulse on dark-adapted leaves, FM′ is the maximum fluorescence after applying a light saturation pulse on light-adapted leaves, Fs is the stationary fluorescence for light-adapted leaves. The fluorometer allows application of far red light for preferential excitation of PSI, for the accurate determination of the minimum fluorescence F0′.

non-photochemical quenching, q_{NP} ($(F_M\text{-}F_M')/(F_M\text{-}F_0)$). More details on these parameters can be found in references [38–41].

2.7. Plant leaves. Fast chlorophyll fluorescence induction curve (OJIP)

Fast chlorophyll fluorescence induction curves (OJIP) were obtained with a Plant Efficiency Analyser (Handy-PEA, Hansatech Instruments Ltd., UK) on previously dark-adapted leaves [37]. Measurements were carried out without detaching the leaves from the plant. Fluorescence was recorded for 1 second while illuminating with saturating light (PPFD = 3,000 μmol m^{-2} s^{-1}). Several photosynthetic parameters were calculated from these measurements. (See Appendix, Table A.1). More details on these parameters can be found in references [42–44].

2.8. Plant leaves. Spectral distribution of initial fluorescence. Correction for light re-absorption processes

Initial fluorescence spectra of the adaxial (upper) face of the dark-adapted leaves were carried out in front-face geometry by means of a steady state spectrofluorometer (QuantaMaster, PTI-Photon Technology International-Brunswick, USA) at room temperature. Several leaves were stacked in groups of three or four in order to assure zero transmittance through them (a necessary condition to apply the correction for light re-absorption processes). The excitation wavelength was set at 460 nm and the emission between 600 and 800 nm was recorded and corrected by the response of the detector at each wavelength. The intensity of the excitation beam was kept sufficiently low, so that successive recordings of fluorescence spectra did not show variations for the ratio of the fluorescence peaks in the red and far-red. In this way, we could assure that appreciable induction of variable chlorophyll fluorescence was absent.

Experimental spectra were then corrected by light re-absorption processes [45,46] by dividing them by the gamma function (Eqs. (6)-(8))

$$I_f^c(\lambda) = \frac{I_f^e(\lambda)}{\gamma(\lambda, \lambda_0)} \tag{6}$$

$$\gamma(\lambda, \lambda_0) = \frac{1}{1+\sqrt{\frac{F(R_\lambda)}{F(R_\lambda)+2}}} \cdot \frac{1}{1+\sqrt{\frac{F(R_\lambda)(F(R_\lambda)+2)}{F(R_{\lambda_0})(F(R_{\lambda_0})+2)}}} \tag{7}$$

where $F(R_\lambda)$ is the remission function at wavelength λ, calculated by Eq. (8) from the diffuse reflectance ($R(\lambda)$) of a thick layer of leaves.

$$F(R_\lambda) = \frac{(1-R_\lambda)^2}{2R_\lambda} \tag{8}$$

In Eq. (7), λ and λ_0 state for emission and excitation wavelengths respectively.

2.9. Statistics

Data processing was carried out in Python using the Numpy module and Pandas, mainly. The statistical analysis was performed using one-way ANOVA with a Tukey HSD post-hoc test (rejection level of 1 and 5%), to determine the statistical significance between groups. For this purpose, Pingouin package was used.

3. Results and discussion

3.1. Properties of nanoparticles

IR spectra for nano-CB and for GQD are shown in Fig. 2. From these results, characteristic signals of the nanoparticles and their respective precursors (not observed in the base signal of the support used) could be distinguished.

Identifying signals corresponding to amide functional groups and C=C bonds in GQD is particularly interesting. In fact, GQD presented a deep and wide band around 1650 cm^{-1}, which is unfolded. In this spectral region, absorption due to C=O stretches of primary amides (-CO-NH-) and C=C stretches of conjugated double bonds usually appears [32,47]. Given the characteristics of the observed band, it is possible that both overlapping signals are present. In addition, peaks located at 1230 and 825 cm^{-1} correspond to stretching of -O-C-O groups, whereas those located at 1400 and 1100 cm^{-1} are associated with C-O stretching of carboxylic -COOH groups [47,48]. Additionally, the bands around 2900 cm^{-1} correspond to aromatic =C-H stretching, commonly observed in graphene-based carbon nanoparticles. Finally, the peak observed at 3300 cm^{-1} is intense and deep, so it could correspond to an N-H or COOH stretch with H bound by a hydrogen bond [47,49]. In this way, we could identify specific functional groups of graphene quantum dots, such as amide groups, carboxyl groups and carbon-carbon double bonds.

On the other hand, the infrared spectrum of nano-CB significantly differed from the spectrum of GQD. Peaks observed at 615 (sharp), 690, 835 and 910 cm^{-1} correspond to signals from an aromatic nucleus. The

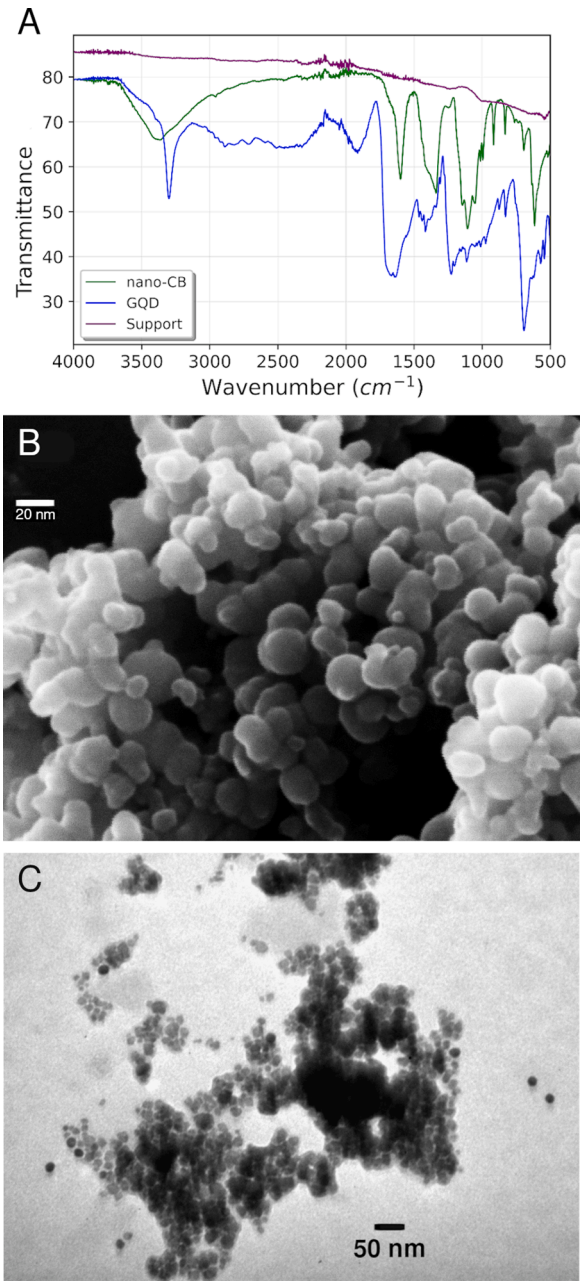

Fig. 2. A) FTIR spectrum for carbon nanoparticles: nano-CB (green line) and GQD (blue line). The sample support spectrum (violet line) is also shown. B) SEM image for nano-GB. C) TEM image for GQD.

strong band at 1100 cm^{-1} is related to stretching of carboxyl C-O-C or C-OH epoxide groups [47–49]. This band is divided into three, and shows the presence of multiple C-O bonds in the sample. The absorption located between 1330 and 1400 cm^{-1} is a deep, wide and asymmetric band, and can be attributed to C-OH and O-H stretching [47,50]. The peak at 1600 cm^{-1} corresponds to C-C stretching of aromatic or polycyclic aromatic groups which is characteristic of carbon dots [32,47,48,51]. Finally, a broad band around 3400 cm^{-1}, characteristic of O-H stretching, was observed.

Thus, from the infrared spectra, the main functional groups present in both nanoparticles could be identified. Whereas in the GQD sample signs of amide groups, carboxylic acid and carbon-carbon bonds were observed, in the nano-CB sample, evidences of aromatic groups, groups with varied C-O bonds and alcohols were noticed. The presence of groups containing oxygen and nitrogen explains the high stability of suspensions of both nanoparticles in water. In general, the IR absorption bands are similar to those previously published in references for this type of carbon nanoparticles [47,48,52–54].

The morphology of the obtained GQDs and nano-CBs was characterized by electron microscopy (Fig. 2. B and C). The average diameter for GQD was 6 ± 1 nm, according to the statistical calculation of more than 300 points (Fig. 2C). Similarly, the average nano-CB size was 12 ± 4 nm. Size and shape distribution was uniform for GQD, whereas nano-CB presented a spherical uniform shape but with a wide size distribution.

Regarding UV-visible spectra, nano-CB presented decreasing absorption from 250 to 600 nm with a slight maximum at 370 nm (Fig. 3A). Given these characteristics, nano-CB spectrum was deconvoluted into three bands, with estimated maxima at 221, 278 and 342 nm. GQD absorbance spectrum, in contrast, showed sharper and better-defined maxima (Fig. 3C). The absorbance spectrum for GQD displayed a typical band around 250 nm and a long tail with a relative maximum at 320 nm, which may be attributed to ππ*of aromatic sp^2 and nπ* (in sp^2 C=O bonds), respectively [48]. For nano-CB, the 221 nm bands could be due to solvent or impurities, while absorptions at 278 and 342 nm are consistent with the two bands observed in the excitation spectra. As in GQD, the bands observed in nano-CB correspond to ππ* and nπ* transitions.

Both nano-CB and GQD are fluorescent. Fluorescence excitation spectra (with emission detection at 440 nm) presented two peaks at 310 and 370 nm for nano-CB and at 279 and 360 nm for GQD (Fig. 3A and 3C, respectively). Fluorescence emission (excited at 360 nm) was observed from 400 to 520 nm for nano-CB (Fig. 3A) and from 380 to 520 nm for GQD (Fig. 3C). Emission maxima are placed at 440 and 425 nm for nano-CB and for GQD, respectively. Excitation-emission matrices are displayed in Fig. 3B and 3D. The fluorescent emission behavior was found to be dependent on the excitation wavelength, which is typical for most fluorescent carbon nanoparticles. Different authors have suggested that such behavior may result from the wide distributions of differently sized dots and surface chemistry, different emissive traps (solvation effect), or a mechanism currently unresolved [15]. In this case, as it can be observed in Fig. 3C and 3D, the emission maximum shift is more evident for nano-CBs. This could indicate that nano-CBs have a broader particle size distribution than GQD [55].

In literature, the blue emission from carbon nanoparticles was attributed to hole-electron recombination or quantum confinement effect, due to the nanoscopic size of the particles [48].

While differences in excitation and emission were observed in similar wavelength ranges for both nano-CB and GQD, their fluorescence quantum yields resulted quite different. In fact, using Rhodamine 101 in ethanol ($\Phi_f = 1.00 \pm 0.05$) as reference, the obtained values were: Φ_f nano-CB = 0.04 ± 0.01 and Φ_f GQD = 0.25 ± 0.05. The values obtained for GQD are similar to those reported in literature for graphene quantum dots of similar composition, spectroscopy and size [48,54,56]. However, the fluorescent quantum yield for nano-CBs was lower than expected for carbon dots. In the reference used for the synthesis of nano-CB, Ye *et al.* [30] also synthesized carbon nanoparticles from an oxidized carbon precursor such as coal and coke. They obtained nanoparticles with low fluorescence quantum yield and with poorly defined band absorption spectra as those observed here. Similarly, other authors who synthesized carbon nanoparticles from candle soot or similar, obtained very small particles of 2 - 6 nm, with low fluorescence quantum yield in the range of 0.008 - 0.12 [28,29,57]. Therefore, the low fluorescence quantum yield obtained for nano-CBs is comprised within the expected range for carbon nanoparticles synthesized from carbon compounds resulting from the combustion of organic matter.

According to the position of the excitation and emission maxima for both nanoparticles, and compared with multiple bibliographical references, the observed spectroscopic characteristics are in line with the sizes obtained by electronic microscopies [16,48]. Finally, Shamsipur *et al.* [58], observed that the smaller the particle size, the greater the

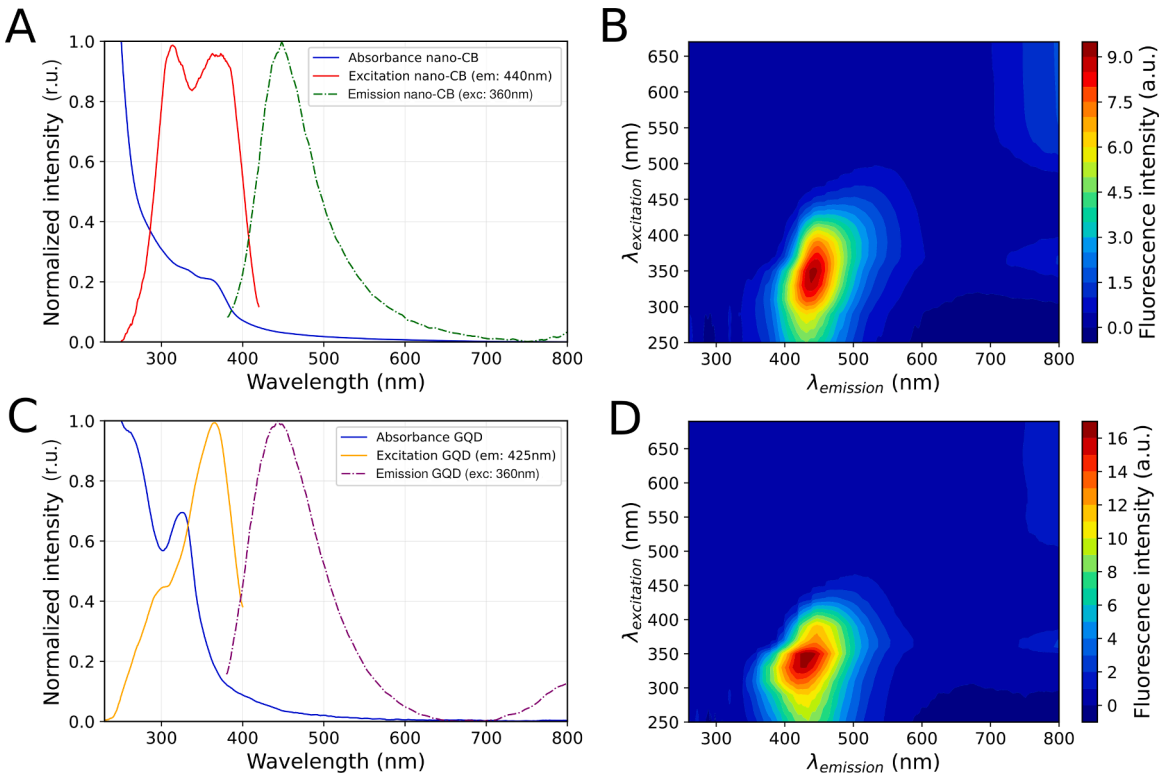

Fig. 3. Nanoparticles characterization. A) Nano-CB. Absorbance, fluorescence excitation (lem: 440 nm) and emission spectra (lexc: 360 nm). B) Nano-CB. Excitation - emission matrices. C) GQD. Absorbance, fluorescence excitation (lem: 440 nm) and emission spectra (lexc: 360 nm). D) GQD. Excitation - emission matrices.

dependence of the emission on the excitation wavelength, and the lower the fluorescence quantum yield of the particles. These features are observed in nano-CBs compared to GQDs, suggesting a smaller mean particle size, a larger particle size distribution, together with a lower quantum yield.

3.2. *Photosynthetic properties of plants treated with nanoparticles*

The results shown below correspond to control and Nps-treated leaves, after four weeks of treatment (sprayed once a day and twice a week during that period of time, as described in Section 2.3).

Leaves treated with either nano-CB or GQD showed a decrease in total chlorophylls, carotenoids and in the ratio Chlorophyll a/b, when compared to those from control plants. An increase in the ratio Chlorophyll/Carotenoids was also evident (Table 1).

It is well known that Chl b is found exclusively in the light harvesting complex (LHC), while Chl a is present in the reaction centers (RC-PSI and RC-PSII) and light harvesting complexes (LHC-I and LHC-II) of both photosystems. While Chl a/b for LHC-I is about 3, the ratio for LHC-II varies from 1.1 to 1.3. As shade plants have much higher amounts of LHC-II than sun-exposed plants, the first type of leaves usually display lower Chl a/b ratios [59,60]. A decrease in the Chl a/b ratio such as that observed here could, therefore, be interpreted as an enlargement of the PSII antenna system due, in principle, to a possible shading effect by nanoparticls presence. Nevertheless, since the UV emission for the used illumination source is practically negligible and the visible light absorption by Nps (although not null) is very low, this shading effect should not be important.

In our study, carotenoid content reduction upon nanoparticles addition was sharper than chlorophyll decrease, so a net increase resulted in the ratio Chls/Cars. This ratio usually varies from 4,2 to 5,0 for sun leaves and from 5,5 to 7,0 for shaded leaves [34].

In summary, the variations observed for pigment content, and Chl a/b and Chls /Cars are similar to those found for shade leaves, but significant shading effects of Nps are here difficult to be justified.

Reflectance indexes, frequently used for plant health assessment, are shown in Table 2. Original reflectance spectra are also displayed in Fig. A1 in the Appendix. NDVI index is empirically related to the green cover of an area and to chlorophyll content of leaves [61]. In our case, even when a decrease in the average value for the leaves treated with nanoparticles (Np-leaves) exists, this is not significant. A statistically significant decrease was observed for mNDVI in agreement with the lower chlorophyll content obtained for Np-leaves. In fact, this spectral index compensates for surface specular reflectance effects of the leaves. The specular component, which is unrelated to pigment concentration,

Table 1
Pigment content expressed per leaf area (μg.cm^{-2}) and pigment ratios, for control and Nps-leaves samples.

Pigments	Control	nano-CB	GQD
Chl a	24.3 ± 2.6*	19.7 ± 2.7*	19.0 ± 2.2*
Chl b	8.8 ± 0.9	7.6 ± 1.2	7.6 ± 0.7
Chl a + b	33 ± 3*	27 ± 4	27 ± 2
Carotenoids	5.4 ± 0.6*	4.1 ± 0.5*	4.0 ± 0.5*
Ratios			
Chl a/b	2.77 ± 0.01*	2.6 ± 0.1	2.47 ± 0.06*
Chl a+b / Cars	6.08 ± 0.01*	6.6 ± 0.2*	6.6 ± 0.2*

* Significant difference, $\alpha < 0.05$.

Table 2
Reflectance indexes for control and Nps-leaves samples.

Spectral index	Control	nano-CB	GQD
NDVI	0.78 ± 0.02	0.77 ± 0.01	0.76 ± 0.01
PRI	0.027 ± 0.003	0.015 ± 0.006	0.013 ± 0.008
mNDVI	0.58 ± 0.02	0.53 ± 0.02*	0.54 ± 0.03
PSNDa	0.81 ± 0.01*	0.80 ± 0.01	0.79 ± 0.01*
PSNDb	0.77 ± 0.02	0.76 ± 0.01	0.75 ± 0.01

* Significant difference, $\alpha < 0.05$.

tends to raise the total reflectance across the visible spectrum and distorts the correlations with pigment content. As Eq. 2 shows, this compensation is mathematically achieved by subtracting the reflectance at 445 nm in the denominator. This index has traditionally displayed better correlations with total chlorophyll content than others [61].

PRI gives information on short-term fluctuations in the levels of pigments in the xanthophyll cycle and thus serves as an estimate of pigments (carotenoids) in the xanthophyll cycle and also of the photosynthetic light use efficiency [61]. PRI values decreased in the leaves treated with nanoparticles with respect to the control, a fact that is consistent with their lower carotenoid content. This suggests a reduced xanthophyll cycle for Nps-leaves, and a consequent lower ability to dissipate excess energy by this pathway. Several authors in literature [62–65] have reported relations between PRI and heat dissipation by NPQ.

Finally, PSNDa and PSNDb are related to the contents of Chl a and Chl b, respectively. The decrease in both indexes observed for Np-leaves accordingly agrees with Chl a and Chl b variations. Although such changes are subtle, it is important to notice that GQD effects are more significant than nano-CBs.

In summary, the variations in the spectral indexes agree with the alterations in pigment composition. Indexes mNDVI, PSNDa and PRI wereg the most sensitive ones.

Fig. 4 (A, B and C) displays the energy partition between photosynthesis (Φ_{PSII}), heat dissipation by non-photochemical quenching (Φ_{NPQ}) and photophysical decay (Φ_c). These three parameters are related and sum to unity since the energy absorbed by PSII is assumed to be able to follow three pathways: it can be dissipated by photophysical processes (intrinsic heat and fluorescence); it can induce the photosynthesis process, by reducing the first electron acceptor; or it can initiate physiological processes that facilitate the release of excess energy in the form of heat (collectively referred to as non-photochemical quenching).

Fig. 4 D and E show, respectively, the coefficients for photochemical and non-photochemical quenching.

As a general observation, it could be noticed that increasing actinic light enhanced the fraction of energy dissipated as heat (Φ_{NPQ}) at the expense of a decrease in the fraction used for photosynthesis (Φ_{PSII}), which is a well-known and expected result for conventional leaves. However, differences between Nps-leaves and control leaves were evident.

At low actinic illumination, PPFD = 12 μmol. $m^{-2}s^{-1}$, the nanoparticle-treated leaves showed a significant increase of Φ_{NPQ} with a reduction of Φ_{PSII} while keeping Φ_C constant. This indicates that the Nps-leaves, at low light intensities, required to dissipate excess energy through NPQ mechanisms, unlike the control. This is a rather surprising behavior since at low AL, the proportion of excited reaction centers is low and dissipation mechanisms such as NPQ should not be necessary. At intermediate AL, the samples and the control displayed similar Φ_{NPQ}. The behavior was reversed at high AL intensity, where the Nps-leaves presented significantly lower Φ_{NPQ} than the control. The response of this parameter for the treated leaves is very similar to that observed in plants acclimatized to low irradiance.

Because NPQ is one of the main mechanisms used by higher plants to cope with excess light, the light response of NPQ reflects the saturation of the photosynthetic rate, increasing rapidly when net photosynthesis per absorbed photon saturates [66–68]. However, the increase in NPQ is limited by the intrinsic capacity of the leaf to dissipate this excess light as heat. For example, Serôdio and Lavaud (2011) [68] reported that plants grown under high irradiance conditions developed a larger pool of xanthophylls to dissipate more excess light energy, compared to plants grown under low or intermediate illumination [66,68] or intermediate illumination [66,68–70]. As a result, NPQ saturates at lower levels of AL in plants grown under intermediate-low light compared to plants grown in high light. The direct relationship between NPQ and the

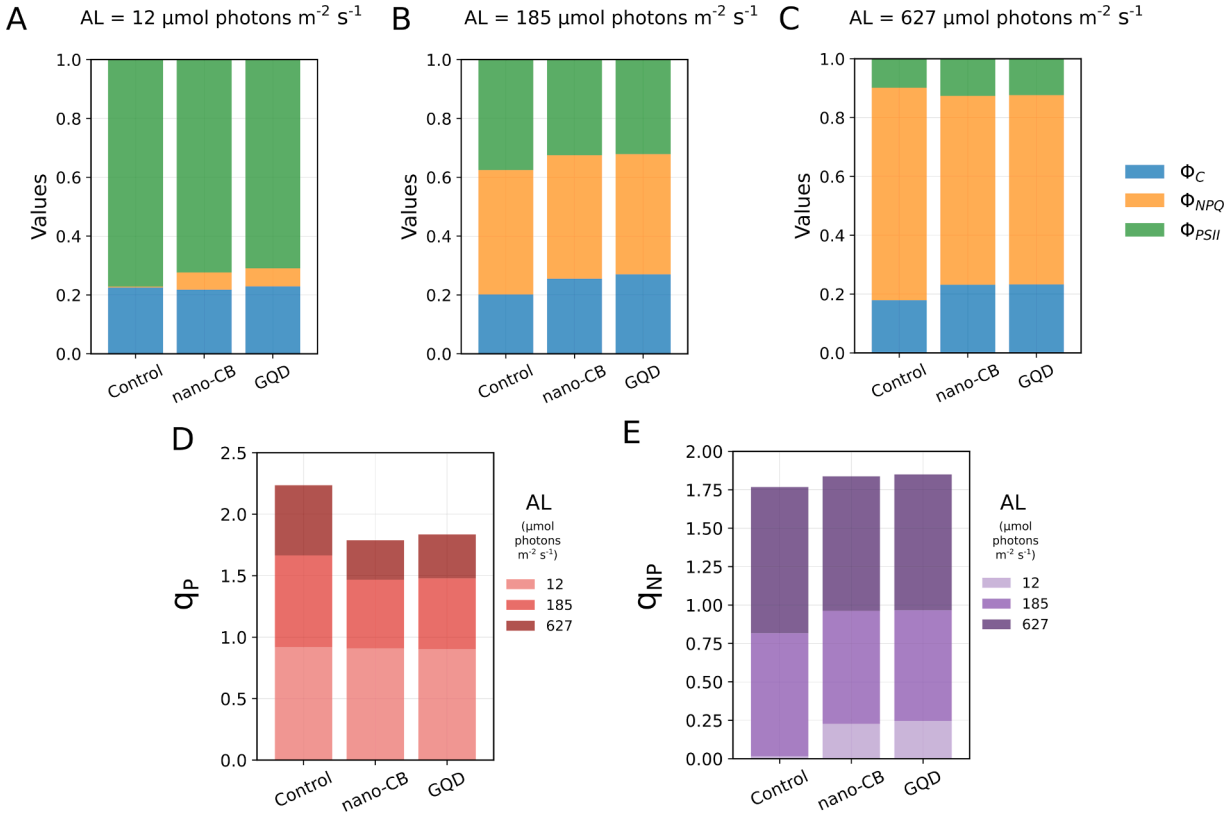

Fig. 4. Photosynthetic parameters and energy partition at different intensities of actinic light (AL). Energy partition between photosynthesis (FPSII), heat dissipation by non-photochemical quenching (FNPQ) and photophysical decay (Fc) under AL with PPFD = 12 mmol . s−1.m−2 (A), Al with PPDF= 185 mmol . s−1.m−2 (B) and Al with PPDF= 627 mmol . s−1.m−2 (C). Coefficients for photochemical, qP (D) and non-photochemical, qNP (E) quenching.

cycle and xanthophyll content is well reported [71,72]. The behavior of NPQ as a function of LA intensity in plants acclimated to different light intensity has been reported previously [68,73]. Thus, it can be argued that the lower NPQ observed in Np-leaves at high AL is not really due to an increase in the photosynthetic efficiency but to a lower pool of xanthophylls. This finding is consistent with the results obtained for pigment content (especially carotenoids) and spectral indexes (in particular PRI), which specifically pointed to a reduced xanthophyll cycle.

Another significant difference between control and Nps-leaves is found in the coefficient for photochemical quenching (q_p), which was considerably lower for Nps-treated leaves at high intensities of AL. This coefficient represents the proportion of energy consumed to initiate photosynthesis and is proportional to the fraction of open reaction centers (RC) of PSII at steady state. Low values of q_P indicate that most PSII RCs are closed and their plastoquinone A (Q_A) is in the reduced state [74,75]. On the other hand, values close to 1 for q_P, indicate that Q_A is in the oxidized state and almost all PSII centers are open. As actinic light increases (Fig. 4), the proportion of closed RCs increases and so q_P decreases. Thus, lower q_P values indicate that a higher proportion of the RCs are closed and a higher proportion of Q_A are reduced. This finding would imply that Nps-treated samples saturate the reduction of acceptors more easily (with a lower number of photons).

The whole set of photosynthetic parameters obtained from Kautsky's kinetics can be found inTable A.2 of the Appendix.

It is worth mentioning that the parameter F_v/F_M did not significantly change upon Nps treatment.

The analysis of fast chlorophyll a fluorescence OJIP transient allows

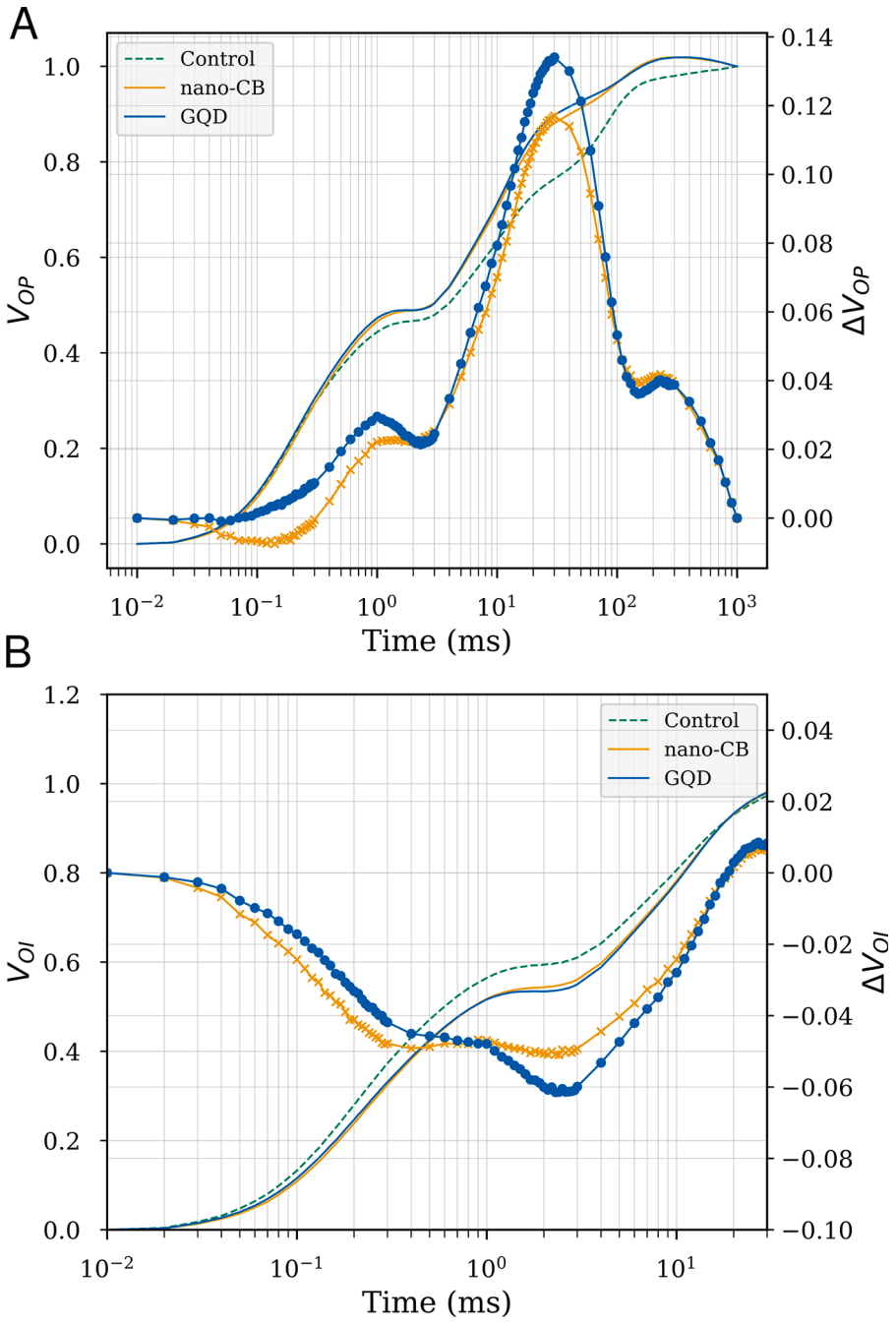

Fig. 5. Normalized OJIP transient for Np-leaves and controls. A: O and P normalization of the OJIP curve (VOP) and kinetic difference of VOP between treatment and control (ΔVOP). B: O and I normalization of the OJIP curve of the OJIP curve (VOI) and kinetic difference of VOI between treatment and control (ΔVOI).

obtaining valuable information on the primary photosynthetic stages. At the F_M level, according to the hypothesis introduced by Duysens and Sweers [76], all Q_A molecules are completely reduced (that is, all active PSII RCs are closed), due to the complete reduction of all the acceptors of electrons from the photosynthetic transport chain, as a result of the applied saturating light pulse. In this way, the different phases of the fluorescence transient (OJ, JI and IP) are due to the progressive saturation of the electron acceptors in the photosynthetic electron transfer chain: OJ follows the reduction of the acceptor side of PSII (Q_A and Q_B); JI represents the reduction of the plastoquinone pool (PQ) and IP parallels the reduction of electron transport acceptors in and around the PSI [77,78]. This means that OJIP transients provide information about the state of electron transport in the photosynthetic chain.

The relative variable fluorescence calculated as $V_{OP} = (F_t - F_0)/(F_P - F_0)$ and the difference VOP = VOP,Np-leaves - VOP,control are shown in Fig. 5A. Magnification of the V_{OI} region is shown in Fig. 5B for more details.

Compared to controls, Chl a fluorescence increased slightly at the J step for Nps-leaves, but this increment was somewhat obscured by the drastic rise observed at the I step. The relative amplitude of the I-P phase followed the decreasing order GQD-leaves > nano-CB-leaves > control. Fig. 5 provides evidence that Nps induced a high increase in the relative variable fluorescence at time I, which is correlated with the fraction of closed PSII centers.

The main photosynthetic parameters (obtained from OJIP curves) for NPs-leaves relative to control values are represented in a spider plot in Fig. 6. The whole set of absolute parameters are shown in Table A.3 in the Appendix. The parameters related to the electron flux in PSII: Φ_{P0} (parameter related to primary PSII photochemistry), Ψ_{Et0} (efficiency with which a PSII trapped electron is transferred from Q_A to Q_B), Φ_{Et0} (quantum yield of electron transport flux from Q_A to Q_B) were kept almost constant upon Nps treatment.

On the other hand, parameters related to PSI activity were seriously affected: δ_{RE}, the efficiency with which an electron can move from the reduced electron acceptors between systems to the PSI electron acceptors; Φ_{RE0}, the quantum yield of electron transport from Q_A^- to the PSI electron acceptors; Ψ_{RE}, the efficiency with which a trapped exciton can move an electron from Q_A^- to the PSI electron acceptors. The reduction in δ_{RE} (around 50% relative to control) is the most meaningful one and strongly suggests that both nano-CB and GQD partially inhibited the activity of PSI. A similar trend was observed in the variations of the specific energy fluxes per RC which include: absorption (ABS/RC), trapping (TR/RC), electron transport (ET/RC), dissipation (DI/RC), and reduction of the final acceptors on the PSI electron acceptor side (RE/RC).

Finally, PI_{ABS} describes the energy conservation between the photons absorbed by PSII and the reduction of inter-system electron acceptors, whereas PI_{ABS}^{total} describes energy conservation between photon absorption and the reduction of the final PSI acceptors [79]. For both nanoparticles, a non-significant increase in PI_{ABS} was observed in parallel to a significant decrease in PI_{ABS}^{total}.

Many studies have used the parameter $F_V/F_M = \Phi_{P0}$, as an indicator of environmental stress [80], but, in recent years, with the impetus given to the recording and interpretation of the OJIP curve, it has been shown that it is an useful indicator whenever the stress does not occur on PSII. For example, in this case, a slight increase was observed in Φ_{P0}, but the overall efficiency of electron transport was drastically reduced by the inhibitory effect on PSI or its acceptors, in agreement with the observed reduction in δ_{RE}, Φ_{RE0}, RE/RC and PI_{ABS}^{total}.

The results show that both types of nanoparticles produced negative and similar changes in the photosynthetic electron transport. The contraction in the Area over the Chl a fluorescence induction curve, accompanied by a reduction in PI_{ABS}^{total}, suggests that PQ pool reduced its size. The findings pointed to a reduction in the efficiency with which an electron can move from the reduced intersystem acceptors to the PSI electron acceptors.

It should be noticed that the variations at the photosynthetic level

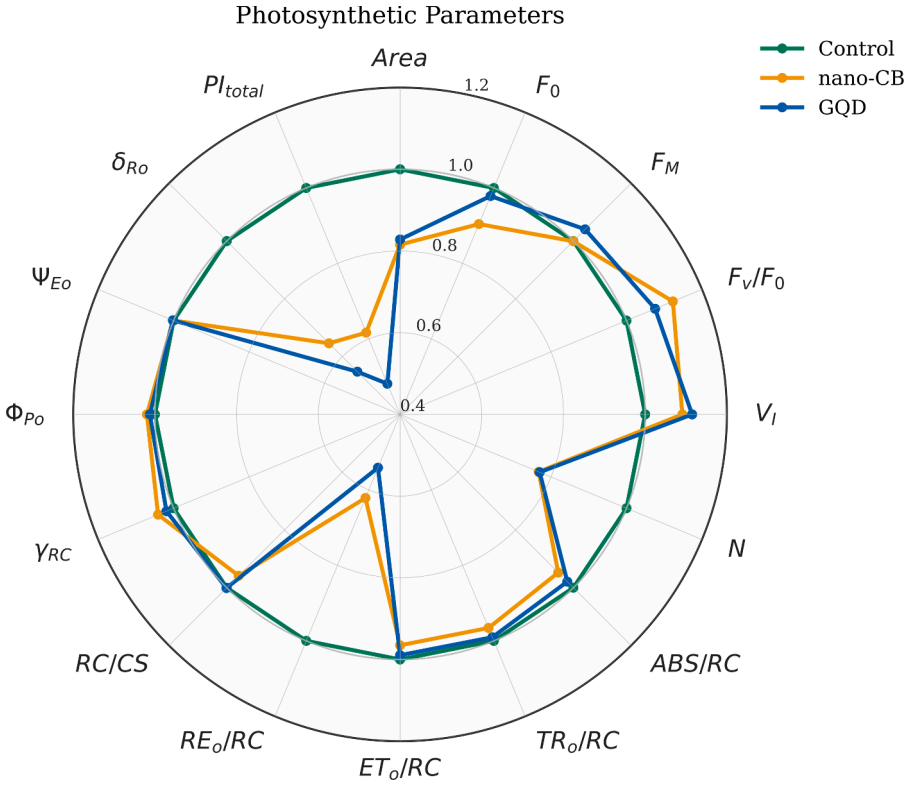

Fig. 6. Relative photosynthetic parameters derived from OJIP curve. Radar plot of selected parameters from OJIP curve. (See the table A1 for the meaning of the symbols and the parameters). All values are shown in relation to control ones (values for control plants = 1).

observed here cannot be attributed to the mere shading effect of the nanoparticles (as suggested for changes in pigment content). In particular, the variations in the parameters Φ_{PO}, Φ_{ET}, Ψ_{ET}, ABS/RC, TR/RC, VJ, among others, did not correspond to acclimatization to low light or shade-grown leaves [81,82]. The yields and quantum efficiencies in each stage of electronic transport were reported to be lower in shaded leaves than in sunny leaves. Our results, on the other hand, showed little or no variations in the parameters associated with PSII, whereas deterioration of the parameters was evident for those related to PSI. Given this fundamental difference, combined with the low light absorption by Nps in the emission region of the light sources, the Nps shadowing hypothesis should be discarded as an important factor.

The fluorescence spectra corrected by the detector response and by light re-absorption processes (according to Section 2.8) are presented in Fig. 7, where normalization at 730 nm was performed. The fluorescence ratios $F_{red}/F_{far\text{-}red}$ were 2.4 ± 0.1, 2.2 ± 0.3 and 2.4 ± 0.3 for control leaves, nano-CB-leaves and GDQ-leaves, respectively, without observing significant differences.

These results allow to assume that no change in the photosystems stoichiometry [83] is induced by Nps presence. A similar result was obtained in literature for plants adapted to suboptimal illumination without modification of the spectral distribution of the exciting light

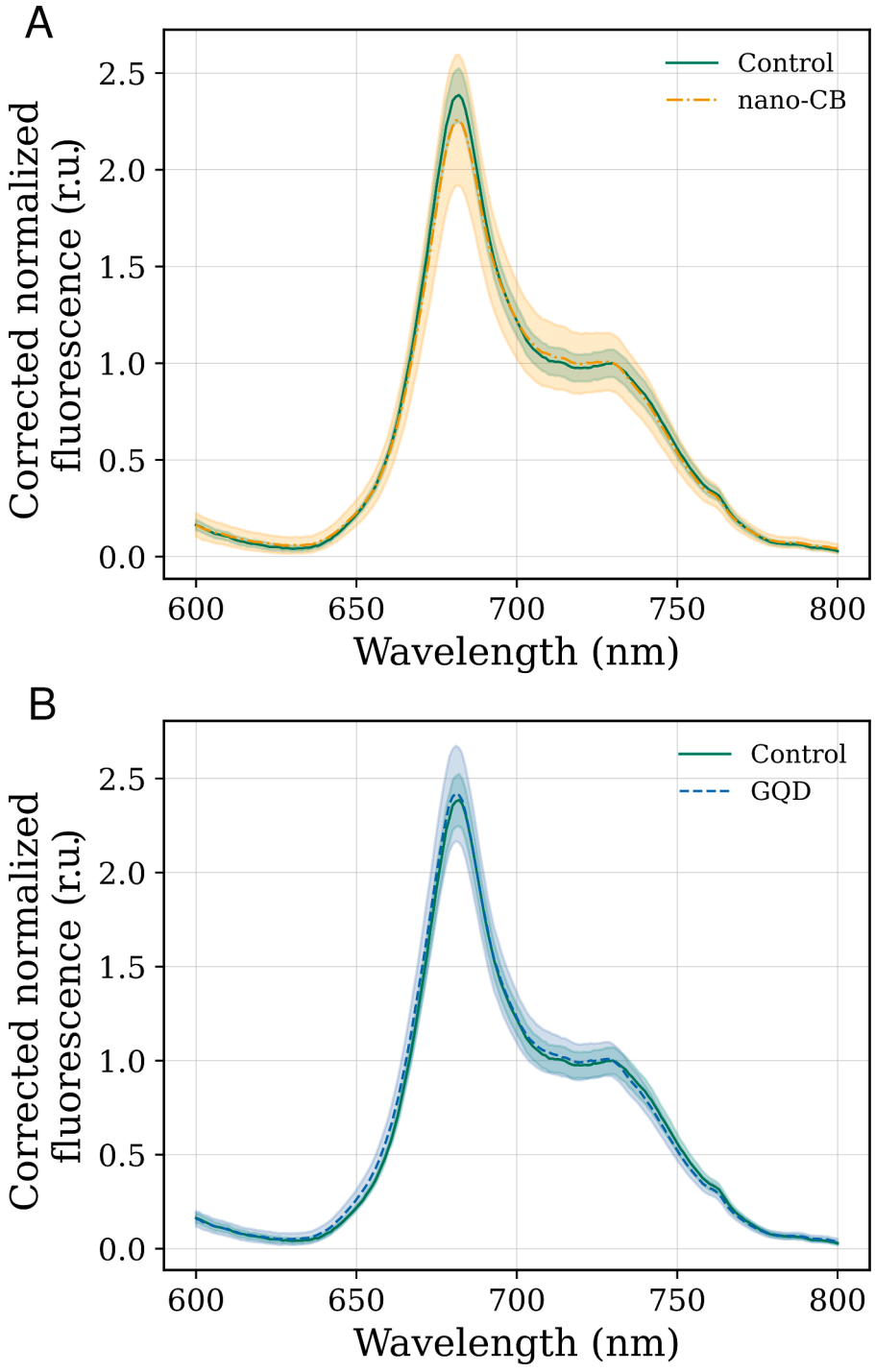

Fig. 7. Fluorescence spectra corrected by light reabsorption, normalized at 730 nm. Spectra for control and for nano-CB-treated leaves (A) and for control and GQD-treated leaves (B).

[40].

When comparing the action of the nanoparticles here synthesized, we find that variations in photosynthetic parameters were more pronounced for GQD than for nano-CB. Although the concentrations used in the treatments were similar for nanoparticles, their sizes and physicochemical properties were different. The greatest effect observed for GQD could possibly be associated with its smaller size and, therefore, with its greater capacity for incorporation into plant tissue. It is also worth noting that GQDs presented higher light absorption and greater light emission than the nanoparticles synthesized from carbon black. A variety of effects of carbon nanoparticles on plants have been reported in literature. Li *et al.* [9] observed positive effects on plant growth at low concentrations (lower or equal to 200 mg/L) and negative consequences at higher concentrations (1000 to 2000 mg/L). Similar results were reported in the review by Mukherjee *et al.* [18]. In the work presented here, the concentrations of the nanoparticles used can be considered high (1 - 2 g/L), and the deterioration observed for the photosynthetic activity for treated leaves are consistent with the reduction in growth described in literature, for such concentration.

The beneficial effects of carbon nanoparticles have been attributed, in bibliography, mainly to two possible mechanisms: antenna effect, in which the nanoparticle absorbs in the UV and transfers energy to the photosystems, and electron transfer processes from the nanoparticles to the chloroplasts [9].

As a matter of fact, fluorescence from carbon nanoparticles can be envisaged as a way to transform ultraviolet radiation into blue light and improve the rate of photosynthesis, by energy transfer to chloroplasts. Nevertheless, unless a light source with a high proportion of UV light is used, it is unlikely to have a significant antenna effect. Even more, the degree of penetration of this radiation in chloroplasts is expected to be small, since outdoor plant leaves usually contain UV screens.

On the other hand, electron transfer processes may be really important and have been suggested as a plausive positive mechanism of action [9]. Our experiments also point to an impact at the level of electron transport, although in this case, it resulted harmful.

A third mechanism of action, presented in iterature showing positive effects, has been related to ribulose-1,5-bisphosphate carboxylase/oxygenase (Rubisco), the main enzyme that assimilates CO_2 in the biosphere [9]. This enzyme has implications in crop yields, nitrogen and water use, and in the global carbon cycle. An increase of 30.9% in Rubisco activity was observed in several plant species such as mung beans, rice, *Trifolium repens L.*, and *Arabidopsis thaliana*, when treated with carbon quantum dots. In fact, it was observed that these quantum dots were degraded by horseradish peroxidase (HRP) and hydrogen peroxide in the plants, a fact that promoted the production of hormone analogues and CO_2. The hormone analogues favoured plant growth, whereas CO_2 was converted to carbohydrates through the Calvin cycle in photosynthesis; both factors favoring plant growth.

Our results indicated that the synthesized carbon nanoparticles interfered with the electron transport chain. More experiments testing the effects of carbon nanoparticles on plants, especially on charge transfer processes, are needed to completely elucidate the possible triggering mechanisms under the observed effects.

4. Conclusions

In this work, we have reported the effect of two types of carbon nanoparticles (nano-CB and GQD) on the photosynthetic machinery of *Cichorium intybus* plant.

Hypothesis i) stating that "Carbon nanoparticles will interfere in the processes of energy and electron transfer within chloroplasts and will have a deleterious effect on photosynthesis" was validated whereas hypothesis ii) was refuted.

The synthesized nanoparticles were found to be fluorescent. Fluorescence efficiency for GQD was over 6 times higher than for nano-CB.

Upon application on leaves, both nanoparticles reduced pigment content. Additionally, Chl a/b decreased and Total Chl/Cars increased. Moreover, experimental evidence suggested a reduced xanthophyll cycle and lower ability to dissipate excess energy by this cycle. The variations in pigment concentration were expressed by the plant through changes in some spectral indexes (mNDVI, PSNDa and PRI).

It was also found that in Nps-treated leaves, saturation of electron acceptors in the photosynthetic chain is attained with a lower number of photons than for control leaves.

Our results suggested that carbon nanoparticles affected the photosynthetic chain at PSI level. The effect was higher for particles with the smallest size.

This work, together with previous literature, shows that further research should be focused on the study of the electron transfer processes taking place in photosynthetic systems containing nanoparticles, to unveil the detailed photophysics describing their mutual interaction.

Declaration of Competing Interest

The authors declare that they have no known competing financial interests or personal relationships that could have appeared to influence the work reported in this paper.

Acknowledgements

This work was supported by the University of Buenos Aires [grant number UBACyT20020170100037BA], by the Agencia Nacional de Promoción Científica y Tecnológica [grant number PICT 2019-2019-01530], by the Organisation for the Prohibition of Chemical Weapons (OPCW, The plant Biomarker challenge) and by CONICET [PIP 2021-2023 GI 11220200101415CO]. MGL is Research Member of CONICET (Argentina). RT developed her work with a CONICET fellowship.

Supplementary materials

Supplementary material associated with this article can be found, in the online version, at doi:10.1016/j.jpap.2022.100121.

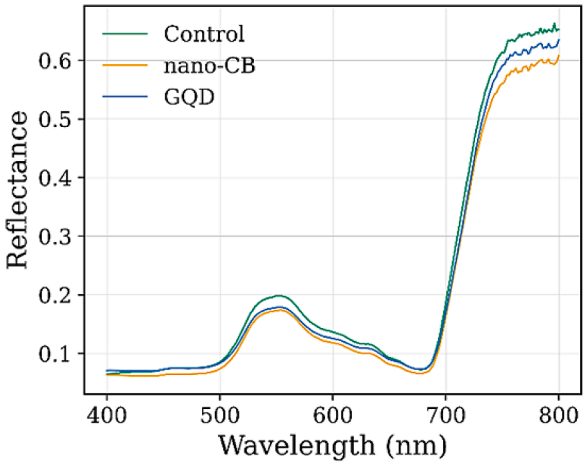

Fig. A1. Reflectance spectra for control leaves (green line), nano-CB treated leaves (orange line) and GQD treated leaves (blue line).

Table A1
Chl fluorescence parameters determined from the Chl fluorescence induction kinetics (based on information presented by Strasser *et. al.* [84], Stirbet *et. al.* [77], and Lichtenthaler *et al.* [39]).

Parameter	Equation	Definition
Common basic parameters of variable fluorescence		
F_o	$F_o = F_{20\ \mu s}$ *or* $F_{50\ \mu s}$	First reliable fluorescence value after the onset of actinic illumination; used as initial value of the fluorescence
F_M	$F_M = F_P$	Fluorescence value at the peak of OJIP curve; maximum value under saturating illumination
$\frac{F_V}{F_M}$	$\frac{F_M - F_O}{F_M}$	* Ratio between variable and maximum fluorescence
$\frac{F_V}{F_o}$	$\frac{F_M - F_O}{F_O}$	Value that is proportional to the activity of the water-splitting complex on the donor side of the PSII
Parameters under actinic illumination (Kautsky'seffect)		
F'_M		Maximum Chl fluorescence in the light-adapted state of leaves (induced by an saturated light)
F_S		Fluorescence level induced by actinic light on stationary state
Φ_C	$\frac{F_S}{F_M}$	Quantum yield of photophysical decay
Φ_{NPQ}	$\frac{F_S\ (F_M - F'_M)}{F_M\ \ F'_M}$	Quantum yield of the NPQ
Φ_{PSII}	$\frac{F'_M - F_S}{F_M}$	Quantum yield of PSII
PS_{rate}	$\Phi_{PSII}\ .\ LA$	Estimated photosynthetic rate of PSII
q_P	$\frac{F'_M - F_S}{F_M - F_o}$	Photochemical quenching of variable Chl fluorescence
q_{NP}	$\frac{F_M - F'_M}{F_M - F_o}$	Non-photochemical quenching of variable Chl fluorescence
Basic JIP-test parameters derived from the OJIP transient		
F_K	$F_{300\ \mu s}$	Fluorescence value at 300 μs
F_J	$F_{2\ ms}$	Fluorescence value at 2 ms (J-level)
F_I	$F_{30\ ms}$	Fluorescence value at 30 ms (I-level)
V_t	$\frac{F_T - F_o}{F_M - F_o}$	Relative variable Chl fluorescence
Area		Area between OJIP curve and the line $F = F_M$
S_M	$\frac{Area}{F_M - F_0}$	Normalized area (related to the number of electron carriers per electron transport chain)
M_O	$4\ ms^{-1}\ \frac{F_K - F_o}{F_M - F_O}$	Approximate value of the initial slope of relative variable Chl fluorescence curve Vt (for Fo = F50μs)
N	$S_M \frac{V_J}{M_O}$	Number indicating how many times Q_A is reduced while fluorescence reaches its maximal value (number of Q_A redox turnovers until Fm is reached)
Quantum yields and probabilities derived from the OJIP transient		
Φ_{PO}	$\frac{TR_o}{ABS} = 1 - \frac{F_o}{F_M}$	*Parameter related to primary PSII photochemistry
Ψ_{ET}	$\frac{ET}{TR_o} = 1 - V_J$	Efficiency/probability with which a PSII trapped electron is transferred from Q_A to Q_B
Φ_{ET}	$\frac{ET}{ABS} = \Phi_{PO}\ (1 - V_J)$	Quantum yield of the electron transport flux from Q_A to Q_B
δ_{RE}	$\frac{RE}{ET} = \frac{1 - V_I}{1 - V_J}$	Efficiency/probability with which an electron from Q_B is transferred until PSI acceptors
Φ_{RE}	$\frac{RE}{ABS} = \Phi_{PO}\ (1 - V_I)$	Quantum yield of the electron transport flux until the PSI electron acceptors
Specific energy fluxes expressed per active PSII reactioncenter(RC)		
$RC\ /ABS$	$\Phi_{PO} \frac{V_J}{M_O} = \frac{\gamma_{RC}}{1 - \gamma_{RC}}$	Number of Q_A reducing RCs per PSII antenna Chl
$ABS\ /RC$	$\frac{M_O}{V_J} \frac{1}{\Phi_{PO}}$	Average absorbed photon flux per PSII reaction center (or also, apparent antenna size of an active PSII)
$TR\ /RC$	$\frac{M_O}{V_J}$	Maximum trapped exciton flux per PSII
$ET\ /RC$	$\frac{M_O}{V_J}\ (1 - V_J)$	Electron transport flux from Q_A to Q_B per PSII
$RE\ /RC$	$\frac{M_O}{V_J}\ (\ 1 - V_I)$	Electron transport flux until PSI acceptors per PSII
$RC\ /CS$	$\frac{RC}{ABS} \frac{ABS}{CS}$	The number of active PSII RCs per cross section
γ_{RC}	$\frac{Chl_{RC}}{Chl_{tot}}$	Probability that a PSII Chl functions as RC
''Performance'' indexes (combination of parameters)		
PI^{ABS}	$\frac{\gamma_{RC}}{1 - \gamma_{RC}}\ \frac{\Phi_{PO}}{1 - \Phi_{PO}}\ \frac{\Psi_{ET}}{1 - \Psi_{ET}}$	Performance index for energy conservation from photons absorbed by PSII antenna, to the reduction of Q_B
PI^{ABS}_{total}	$PI^{ABS} \frac{\delta_{RE}}{1 - \delta_{RE}}$	Performance index for energy conservation from photons absorbed by PSII antenna, until the reduction of PSI acceptors

* Φ_{PO} and F_v/F_M have been previously considered in literature as the maximum quantum yield of photosynthesis for dark-adapted leaves. A very recent research has shown that although these parameters are related to PSII activity, they cannot be strictly considered as the maximum quantum yield of photosynthesis [85].

Table A2
Additional parameters derived from Kautsky kinetic.

Parámetros	AL	Control	nano-CB	GQD
F_o	-	205 ± 19	202 ± 14	211 ± 18
F_M	-	1300 ± 88	1259 ± 84	1252 ± 137
F_V	-	1094 ± 72	1056 ± 72	1042 ± 124
F_V/F_M	-	0.84 ± 0.01	0.84 ± 0.00	0.83 ± 0.01
F_V/F_o	-	5.3 ± 0.3	5.2 ± 0.2	5.0 ± 0.4
F_M'	10	1281 ± 66*	1020 ± 178*	995 ± 143*
	25	424 ± 77	484 ± 78	500 ± 140
	40	260 ± 45	335 ± 38	330 ± 35
F_S	10	293 ± 35	274 ± 21	285 ± 24
	25	263 ± 34*	321 ± 29	336 ± 82*
	40	234 ± 37*	291 ± 29*	289 ± 34*
Φ_C	10	0.23 ± 0.02	0.22 ± 0.01	0.23 ± 0.02
	25	0.20 ± 0.02*	0.26 ± 0.01	0.27 ± 0.07*
	40	0.18 ± 0.02*	0.23 ± 0.01*	0.23 ± 0.04*
Φ_{NPQ}	10	0.00 ± 0.01*	0.06 ± 0.05	0.06* ± 0.03*
	25	0.42 ± 0.06	0.42 ± 0.09	0.41 ± 0.09
	40	0.72 ± 0.03*	0.64 ± 0.04*	0.64 ± 0.03*
Φ_{PSII}	10	0.77 ± 0.02*	0.72 ± 0.05	0.71 ± 0.04*
	25	0.38 ± 0.05	0.33 ± 0.09	0.32 ± 0.07
	40	0.10 ± 0.02	0.13 ± 0.04	0.12 ± 0.03
PS_{rate}	10	9.3 ± 0.2*	8.7 ± 0.6	8.5 ± 0.4*
	25	63 ± 11	80 ± 23	79 ± 16
	40	62 ± 11	80 ± 22	78 ± 16
q_P	10	0.92 ± 0.02	0.91 ± 0.02	0.90 ± 0.02
	25	0.75 ± 0.05*	0.56 ± 0.11*	0.58 ± 0.10*
	40	0.57 ± 0.20*	0.32 ± 0.07*	0.36 ± 0.10*
q_{NP}	10	0.02 ± 0.05*	0.23 ± 0.15*	0.25 ± 0.10*
	25	0.80 ± 0.06	0.73 ± 0.06	0.72 ± 0.12
	40	0.95 ± 0.03*	0.88 ± 0.03*	0.88 ± 0.04*

* Significant difference, $\alpha < 0.05$.

Table A3
Additional parameters derived from OJIP transient.

Parameter	Control	nano-CB	GQD
F_o	433 ± 32	391 ± 35	423 ± 22
F_M	2495 ± 149	2494 ± 268	2596 ± 99
F_J	1458 ± 56	1435 ± 132	1503 ± 80
F_I	2071 ± 124 *	2215 ± 236 *	2349 ± 81 *
F_V/F_M	0.83 ± 0.01 *	0.84 ± 0.01 *	0.84 ± 0.01
F_V/F_o	4.8 ± 0.4 *	5.4 ± 0.4 *	5.1 ± 0.4
V_K	0.32 ± 0.03	0.31 ± 0.04	0.32 ± 0.05
V_J	0.50 ± 0.02	0.50 ± 0.03	0.50 ± 0.03
V_I	0.80 ± 0.03 *	0.87 ± 0.02 *	0.89 ± 0.02 *
N	44 ± 2 *	34 ± 2*	34 ± 3 *
S_M	20 ± 1 *	16 ± 1 *	16 ± 2 *
Area	(4.2 ± 0.5) 10^5 *	(3.4 ± 0.6) 10^5 *	(3.5 ± 0.6) 10^5 *
M_o	1.1 ± 0.1	1.0 ± 0.1	1.1 ± 0.1
Φ_{PO}	0.83 ± 0.01 *	0.84 ± 0.01 *	0.84 ± 0.01
Ψ_{ET}	0.50 ± 0.03	0.50 ± 0.03	0.50 ± 0.03
Φ_{ET}	0.41 ± 0.03	0.42 ± 0.03	0.42 ± 0.03
δ_{RE}	0.41 ± 0.06 *	0.26 ± 0.05 *	0.22 ± 0.04 *
Φ_{RE}	0.17 ± 0.03 *	0.11 ± 0.02 *	0.09 ± 0.02 *
RC/ABS	0.38 ± 0.02	0.40 ± 0.03	0.39 ± 0.04
ABS/RC	2.6 ± 0.1	2.5 ± 0.2	2.6 ± 0.2
TR/RC	2.1 ± 0.1	2.1 ± 0.1	2.1 ± 0.2
ET/RC	1.11 ± 0.08	1.05 ± 0.07	1.07 ± 0.08
RE/RC	0.44 ± 0.07 *	0.27 ± 0.05 *	0.24 ± 0.04 *
RC/CS	166 ± 19	159 ± 23	166 ± 14
γ_{RC}	0.28 ± 0.01	0.29 ± 0.01	0.28 ± 0.02
PI^{ABS}	1.9 ± 0.3	2.2 ± 0.5	2.1 ± 0.5
PI^{ABS}_{total}	1.3 ± 0.5 *	0.8 ± 0.3 *	0.6 ± 0.3 *

* Significant difference, $\alpha < 0.05$.

References

[1] X.G. Zhu, S.P. Long, D.R. Ort, What is the maximum efficiency with which photosynthesis can convert solar energy into biomass? Curr. Opin. Biotechnol. 19 (2008) 153–159, https://doi.org/10.1016/j.copbio.2008.02.004.

[2] H. El-Ramady, N. Abdalla, T. Alshaal, A. El-Henawy, M. Elmahrouk, Y. Bayoumi, T. Shalaby, M. Amer, S. Shehata, M. Fári, É. Domokos-Szabolcsy, A. Sztrik, J. Prokisch, E.A.H. Pilon-Smits, M. Pilon, D. Selmar, S. Hanekłaus, E. Schnug, Plant nano-nutrition, in: K.M. Gothandam, S. Ranjan, N. Dasgupta, C. Ramalingam, E. Lichtfouse (Eds.), Perspectives and Challenges, Springer International Publishing, Cham, 2018, pp. 129–161, https://doi.org/10.1007/978-3-319-70166-0_4.

[3] S.K. Ghosh, T. Bera, 16 - Unraveling the mechanism of nanoparticles for controlling plant pathogens and pests, in: S. Jogaiah, H.B. Singh, L.F. Fraceto, R. de B.T.-A. in N.-F., N.-P. in A. Lima (Eds.), 16 - Unraveling the mechanism of nanoparticles for controlling plant pathogens and pests, Woodhead Publ. Ser. Food Sci. Technol. Nutr (2021) 415–436, https://doi.org/10.1016/B978-0-12-820092-6.00016-1, https://doi.org/https://doi.org/.

[4] P. Vega-Vásquez, N.S. Mosier, J. Irudayaraj, Nanoscale drug delivery systems: from medicine to agriculture, Front. Bioeng. Biotechnol. 8 (2020), https://doi.org/10.3389/fbioe.2020.00079.

[5] L. Giorgetti, N.K.B.T.-N., Algae and Microorganisms, Effects of nanoparticles in plants: Phytotoxicity and genotoxicity assessment, in: D.K. Tripathi, P. Ahmad, S. Sharma, D.K. Chauhan, P. Dubey (Eds.), Effects of nanoparticles in plants: Phytotoxicity and genotoxicity assessment, Nanomater. Plants, Algae Microorg. Concepts Controv 2 (2018) 65–87, https://doi.org/10.1016/B978-0-12-811488-9.00004-4.

[6] F.N. Spagnoletti, F. Kronberg, C. Spedalieri, E. Munarriz, R. Giacometti, Protein corona on biogenic silver nanoparticles provides higher stability and protects cells from toxicity in comparison to chemical nanoparticles, J. Environ. Manage. 297 (2021), 113434, https://doi.org/10.1016/j.jenvman.2021.113434.

[7] P. Strobbia, R.A. Odion, T. Vo-Dinh, Spectroscopic chemical sensing and imaging: from plants to animals and humans, Chemosensors 6 (2018), https://doi.org/10.3390/chemosensors6010011.

[8] T.R. Shojaei, M.A.M. Salleh, M. Tabatabaei, H. Mobli, M. Aghbashlo, S.A. Rashid, T. Tan, Applications of nanotechnology and carbon nanoparticles in agriculture, Elsevier Inc., 2018, https://doi.org/10.1016/B978-0-12-815757-2.00011-5.

[9] Y. Li, X. Xu, Y. Wu, J. Zhuang, X. Zhang, H. Zhang, B. Lei, C. Hu, Y. Liu, A review on the effects of carbon dots in plant systems, Mater. Chem. Front. 4 (2020) 437–448, https://doi.org/10.1039/C9QM00614A.

[10] M.J. Molaei, Principles, mechanisms, and application of carbon quantum dots in sensors: a review, Anal. Methods. 12 (2020) 1266–1287, https://doi.org/10.1039/c9ay02696g.

[11] S.N. Baker, G.A. Baker, Luminescent carbon nanodots: emergent nanolights, Angew. Chemie Int. Ed. 49 (2010) 6726–6744, https://doi.org/10.1002/ANIE.200906623.

[12] H. Li, Z. Kang, Y. Liu, S.T. Lee, Carbon nanodots: Synthesis, properties and applications, J. Mater. Chem. 22 (2012) 24230–24253, https://doi.org/10.1039/c2jm34690g.

[13] S. Mitra, S. Chandra, P. Patra, P. Pramanik, A. Goswami, Novel fluorescent matrix embedded carbon quantum dots for the production of stable gold and silver hydrosols, J. Mater. Chem. 21 (2011) 17638–17641, https://doi.org/10.1039/C1JM13858H.

[14] L. Cao, S. Sahu, P. Anilkumar, C.E. Bunker, J. Xu, K.A.S. Fernando, P. Wang, E. A. Guliants, K.N. Tackett, Y.P. Sun, Carbon nanoparticles as visible-light photocatalysts for efficient CO2 conversion and beyond, J. Am. Chem. Soc. 133 (2011) 4754–4757, https://doi.org/10.1021/JA200804H.

[15] S. Zhu, Y. Song, X. Zhao, J. Shao, J. Zhang, B. Yang, The photoluminescence mechanism in carbon dots (graphene quantum dots, carbon nanodots, and polymer dots): current state and future perspective, Nano Res. 8 (2015) 355–381, https://doi.org/10.1007/s12274-014-0644-3.

[16] F. Yan, Z. Sun, H. Zhang, X. Sun, Y. Jiang, Z. Bai, The fluorescence mechanism of carbon dots, and methods for tuning their emission color: a review, Microchim. Acta. 186 (2019) 1–37, https://doi.org/10.1007/S00604-019-3688-Y/TABLES/5.

[17] S. Zhu, Q. Meng, L. Wang, J. Zhang, Y. Song, H. Jin, K. Zhang, H. Sun, H. Wang, B. Yang, Highly photoluminescent carbon dots for multicolor patterning, sensors, and bioimaging, Angew. Chemie. 125 (2013) 4045–4049, https://doi.org/10.1002/ange.201300519.

[18] A. Mukherjee, S. Majumdar, A.D. Servin, L. Pagano, O.P. Dhankher, J.C. White, Carbon nanomaterials in agriculture: a critical review, Front. Plant Sci. 7 (2016) 1–16, https://doi.org/10.3389/fpls.2016.00172.

[19] E. Navarro, A. Baun, R. Behra, N.B. Hartmann, J. Filser, A.J. Miao, A. Quigg, P. H. Santschi, L. Sigg, Environmental behavior and ecotoxicity of engineered nanoparticles to algae, plants, and fungi, ecotoxicol. 17 (2008) 372–386, https://doi.org/10.1007/s10646-008-0214-0.

[20] L.R. Khot, S. Sankaran, J.M. Maja, R. Ehsani, E.W. Schuster, Applications of nanomaterials in agricultural production and crop protection: A review, Crop Prot. 35 (2012) 64–70, https://doi.org/10.1016/j.cropro.2012.01.007.

[21] R. Raliya, V. Saharan, C. Dimkpa, P. Biswas, Nanofertilizer for precision and sustainable agriculture: current state and future perspectives, J. Agric. Food Chem. 66 (2018) 6487–6503, https://doi.org/10.1021/acs.jafc.7b02178.

[22] T. Eichert, H.E. Goldbach, Equivalent pore radii of hydrophilic foliar uptake routes in stomatous and astomatous leaf surfaces – further evidence for a stomatal pathway, Physiol. Plant. 132 (2008) 491–502, https://doi.org/10.1111/j.1399-3054.2007.01023.x, https://doi.org/https://doi.org/.

[23] G. Uzu, S. Sobanska, G. Sarret, M. Muñoz, C. Dumat, Foliar lead uptake by lettuce exposed to atmospheric fallouts, Environ. Sci. Technol. 44 (2010) 1036–1042, https://doi.org/10.1021/es902190u.

[24] J. Lv, P. Christie, S. Zhang, Uptake, translocation, and transformation of metal-based nanoparticles in plants: recent advances and methodological challenges, Environ. Sci. Nano. 6 (2019) 41–59, https://doi.org/10.1039/C8EN00645H.

[25] I. Milenković, M. Borišev, Y. Zhou, S.Z. Spasić, R.M. Leblanc, K. Radotić, Photosynthesis enhancement in maize via nontoxic orange carbon dots, J. Agric. Food Chem. 69 (2021) 5446–5451, https://doi.org/10.1021/acs.jafc.1c01094.

[26] S. Chandra, S. Pradhan, S. Mitra, P. Patra, A. Bhattacharya, P. Pramanik, A. Goswami, High throughput electron transfer from carbon dots to chloroplast: A rationale of enhanced photosynthesis, Nanoscale 6 (2014) 3647–3655, https://doi.org/10.1039/c3nr06079a.

[27] J. Chen, R. Dou, Z. Yang, X. Wang, C. Mao, X. Gao, L. Wang, The effect and fate of water-soluble carbon nanodots in maize (Zea mays L, Nanotoxicology 10 (2016) 818–828, https://doi.org/10.3109/17435390.2015.1133864.

[28] S. Hu, Z. Wei, Q. Chang, A. Trinchi, J. Yang, A facile and green method towards coal-based fluorescent carbon dots with photocatalytic activity, Appl. Surf. Sci. 378 (2016) 402–407, https://doi.org/10.1016/j.apsusc.2016.04.038.

[29] S.C. Ray, A. Saha, N.R. Jana, R. Sarkar, Fluorescent carbon nanoparticles: Synthesis, characterization, and bioimaging application, J. Phys. Chem. C. 113 (2009) 18546–18551, https://doi.org/10.1021/jp905912n.

[30] R. Ye, C. Xiang, J. Lin, Z. Peng, K. Huang, Z. Yan, N.P. Cook, E.L.G. Samuel, C. C. Hwang, G. Ruan, G. Ceriotti, A.R.O. Raji, A.A. Martí, J.M. Tour, Coal as an abundant source of graphene quantum dots, Nat. Commun. 4 (2013) 1–7, https://doi.org/10.1038/ncomms3943.

[31] B. Han, M. Yu, T. Pen, Y. Li, X. Hu, R. Xiang, X. Hou, G. He, One-step extraction of highly fluorescent carbon quantum dots by a physical method from carbon black, New J. Chem. 41 (2017) 5267–5270, https://doi.org/10.1039/C7NJ00858A.

[32] X. Wu, F. Tian, W. Wang, J. Chen, M. Wu, J.X. Zhao, Fabrication of highly fluorescent graphene quantum dots using L-glutamic acid for in vitro/in vivo imaging and sensing, J. Mater. Chem. C. 1 (2013) 4676–4684, https://doi.org/10.1039/c3tc30820k.

[33] M. Levitus, Tutorial: Measurement of fluorescence spectra and determination of relative fluorescence quantum yields of transparent samples, Methods Appl. Fluoresc. 8 (2020), https://doi.org/10.1088/2050-6120/ab7e10.

[34] H.K. Lichtenthaler, C. Buschmann, Chlorophylls and carotenoids: measurement and characterization by UV-VIS spectroscopy, Handb. Food Anal. Chem. (2005) 171–178, https://doi.org/10.1002/0471709085.ch21, 2–2.

[35] D.A. Sims, J.A. Gamon, Relationships between leaf pigment content and spectral reflectance across a wide range of species, leaf structures and developmental stages, Remote Sens. Environ. (2002), https://doi.org/10.1016/S0034-4257(02)00010-X.

[36] G.A. Blackburn, Spectral indices for estimating photosynthetic pigment concentrations: a test using senescent tree leaves, Int. J. Remote Sens. 19 (1998) 657–675, https://doi.org/10.1080/014311698215919.

[37] R. Torres, J.M. Romero, M.G. Lagorio, Effects of sub-optimal illumination in plants. Comprehensive chlorophyll fluorescence analysis, J. Photochem. Photobiol. B Biol. 218 (2021), 112182, https://doi.org/10.1016/j.jphotobiol.2021.112182.

[38] B. Genty, J.-M.M. Briantais, N.R. Baker, The relationship between the quantum yield of photosynthetic electron transport and quenching of chlorophyll fluorescence, Biochim. Biophys. Acta (BBA)-General Subj. 990 (1989) 87–92, https://doi.org/10.1016/S0304-4165(89)80016-9.

[39] H.K. Lichtenthaler, C. Buschmann, M. Knapp, How to correctly determine the different chlorophyll fluorescence parameters and the chlorophyll fluorescence decrease ratio RFd of leaves with the PAM fluorometer, Photosynthetica 43 (2005) 379–393, https://doi.org/10.1007/s11099-005-0062-6.

[40] R. Torres, J.M. Romero, M.G. Lagorio, Effects of sub-optimal illumination in plants. Comprehensive chlorophyll fluorescence analysis, J. Photochem. Photobiol. B Biol. 218 (2021), 112182, https://doi.org/10.1016/j.jphotobiol.2021.112182.

[41] J.M. Romero, R. Torres, B. Ospina Calvo, V.E. Diz, A. Iriel, G.B. Cordon, M. G. Lagorio, Photochemistry and photophysics of biological systems. Chlorophyll fluorescence and photosynthesis, J. Argentine Chem. Soc. 106 (2020).

[42] A. Stirbet, Govindjee, Chlorophyll a fluorescence induction: a personal perspective of the thermal phase, the J–I–P rise, Photosynth. Res. 113 (2012) 15–61, https://doi.org/10.1007/s11120-012-9754-5.

[43] R.J. Strasser, A. Srivastava, M. Tsimilli-Michael, Analysis of the fluorescence transiet as a tool to characterize and screen photosynthetic samples, Photosynth. Res. (2004) 445–483, https://pdfs.semanticscholar.org/e1c8/f20e961f2ff50490562eb2ebe119f14a34ee.pdf.

[44] H.M. Kalaji, K. Govindjee, J. Bosa, K. Kościelniak, Żuk-Gołaszewska, Effects of salt stress on photosystem II efficiency and CO 2 assimilation in two syrian barley landraces, Environ. Exp. Bot. 73 (2011) 64–72, https://doi.org/10.1007/978-3-642-32034-7_164.

[45] G.B. Cordón, M.G. Lagorio, Re-absorption of chlorophyll fluorescence in leaves revisited. A comparison of correction models, Photochem. Photobiol. Sci. 5 (2006) 735–740, https://doi.org/10.1039/b517610g.

[46] M.E. Ramos, M.G. Lagorio, True fluorescence spectra of leaves, Photochem. Photobiol. Sci. 3 (2004) 1063–1066, https://doi.org/10.1039/b406525e.

[47] V. Ţucureanu, A. Matei, A.M. Avram, FTIR spectroscopy for carbon family study, Crit. Rev. Anal. Chem. 46 (2016) 502–520, https://doi.org/10.1080/10408347.2016.1157013.

[48] T. Fan, W. Zeng, W. Tang, C. Yuan, S. Tong, K. Cai, Y. Liu, W. Huang, Y. Min, A. J. Epstein, Controllable size-selective method to prepare graphene quantum dots from graphene oxide, Nanoscale Res. Lett. 10 (2015) 1–8, https://doi.org/10.1186/s11671-015-0783-9.

[49] E. Pretsch, P. Bühlmann, M. Badertscher, Structure determination of organic compounds: tables of spectral data, Struct. Determ. Org. Compd. Tables Spectr. Data. (2009) 1–433, https://doi.org/10.1007/978-3-540-93810-1.

[50] H. Zhang, H. Huang, H. Ming, H. Li, L. Zhang, Y. Liu, Z. Kang, Carbon quantum dots/Ag3PO4 complex photocatalysts with enhanced photocatalytic activity and stability under visible light, J. Mater. Chem. 22 (2012) 10501–10506, https://doi.org/10.1039/C2JM30703K.

[51] H. Li, X. He, Z. Kang, H. Huang, Y. Liu, J. Liu, S. Lian, C.H.A. Tsang, X. Yang, S.-T. Lee, Water-soluble fluorescent carbon quantum dots and photocatalyst design, Angew. Chemie Int. Ed. 49 (2010) 4430–4434, https://doi.org/10.1002/anie.200906154, https://doi.org/https://doi.org/.

[52] J. Peng, W. Gao, B.K. Gupta, Z. Liu, R. Romero-Aburto, L. Ge, L. Song, L. B. Alemany, X. Zhan, G. Gao, S.A. Vithayathil, B.A. Kaipparettu, A.A. Marti, T. Hayashi, J.J. Zhu, P.M. Ajayan, Graphene quantum dots derived from carbon fibers, Nano Lett. 12 (2012) 844–849, https://doi.org/10.1021/nl2038979.

[53] H. Baweja, K. Jeet, Economical and green synthesis of graphene and carbon quantum dots from agricultural waste, Mater. Res. Express. 6 (2019), https://doi.org/10.1088/2053-1591/AB28E5, 0850g8.

[54] L. Wang, Y. Wang, T. Xu, H. Liao, C. Yao, Y. Liu, Z. Li, Z. Chen, D. Pan, L. Sun, M. Wu, Gram-scale synthesis of single-crystalline graphene quantum dots with superior optical properties, Nat. Commun. 5 (2014) 1–9, https://doi.org/10.1038/ncomms6357.

[55] J. Yao, M. Yang, Y. Duan, Chemistry, biology, and medicine of fluorescent nanomaterials and related systems: new insights into Biosensing, Bioimaging, genomics, diagnostics, and therapy, Chem. Rev 114 (2014) 6130–6178, https://doi.org/10.1021/cr200359p.

[56] H. Wang, P. Gao, Y. Wang, J. Guo, K.Q. Zhang, D. Du, X. Dai, G. Zou, Fluorescently tuned nitrogen-doped carbon dots from carbon source with different content of carboxyl groups, APL Mater 3 (2015) 1–8, https://doi.org/10.1063/1.4928028.

[57] K. Khatri, M.S. Rathore, Plant nanobionics and its applications for developing plants with improved photosynthetic capacity, Photosynth. - From Its Evol. to Futur. Improv. Photosynth. Effic. Using Nanomater. (2018), https://doi.org/10.5772/INTECHOPEN.76815.

[58] M. Shamsipur, A. Barati, A.A. Taherpour, M. Jamshidi, Resolving the multiple emission centers in carbon dots: from fluorophore molecular states to aromatic domain states and carbon-core states, J. Phys. Chem. Lett. 9 (2018) 4189–4198, https://doi.org/10.1021/ACS.JPCLETT.8B02043/SUPPL_FILE/JZ8B02043_SI_001.PDF.

[59] G. Sarijeva, M. Knapp, H.K. Lichtenthaler, Differences in photosynthetic activity, chlorophyll and carotenoid levels, and in chlorophyll fluorescence parameters in green sun and shade leaves of Ginkgo and Fagus, J. Plant Physiol. 164 (2007) 950–955, https://doi.org/10.1016/j.jplph.2006.09.002.

[60] G. Sarijeva, M. Knapp, H.K. Lichtenthaler, Differences in photosynthetic activity, chlorophyll and carotenoid levels, and in chlorophyll fluorescence parameters in green sun and shade leaves of Ginkgo and Fagus, J. Plant Physiol. 164 (2007) 950–955, https://doi.org/10.1016/j.jplph.2006.09.002.

[61] D.A. Sims, J.A. Gamon, Relationships between leaf pigment content and spectral reflectance across a wide range of species, leaf structures and developmental stages, Remote Sens. Environ. 81 (2002) 337–354, https://doi.org/10.1016/S0034-4257(02)00010-X.

[62] L. Yudina, E. Sukhova, E. Gromova, V. Nerush, V. Vodeneev, V. Sukhov, A light-induced decrease in the photochemical reflectance index (PRI) can be used to estimate the energy-dependent component of non-photochemical quenching under heat stress and soil drought in pea, wheat, and pumpkin, Photosynth. Res. 146 (2020) 175–187, https://doi.org/10.1007/s11120-020-00718-x.

[63] K. Kohzuma, M. Tamaki, K. Hikosaka, Corrected photochemical reflectance index (PRI) is an effective tool for detecting environmental stresses in agricultural crops under light conditions, J. Plant Res. 134 (2021) 683–694, https://doi.org/10.1007/S10265-021-01316-1, 2021 1344.

[64] L. Alonso, S. Van Wittenberghe, J. Amorós-López, J. Vila-Francés, L. Gómez-Chova, J. Moreno, Diurnal cycle relationships between passive fluorescence, pri and NPQ of vegetation in a controlled stress experiment, Remote Sens 9 (2017) 770, https://doi.org/10.3390/RS9080770, 2017, Vol. 9, Page 770.

[65] E. Sukhova, V. Sukhov, Analysis of light-induced changes in the photochemical reflectance index (PRI) in leaves of pea, wheat, and pumpkin using pulses of green-yellow measuring light, Remote Sens 11 (2019) 810, https://doi.org/10.3390/RS11070810, 2019, Vol. 11, Page 810.

[66] A.M. Gilmore, Mechanistic aspects of xanthophyll cycle-dependent photoprotection in higher plant chloroplasts and leaves, Physiol. Plant. 99 (1997) 197–209, https://doi.org/10.1111/J.1399-3054.1997.TB03449.X.

[67] R. Goss, B. Lepetit, Biodiversity of NPQ, J. Plant Physiol. 172 (2015) 13–32, https://doi.org/10.1016/j.jplph.2014.03.004.

[68] J. Serôdio, J. Lavaud, A model for describing the light response of the nonphotochemical quenching of chlorophyll fluorescence, Photosynth. Res. 108 (2011) 61–76, https://doi.org/10.1007/S11120-011-9654-0/FIGURES/6.

[69] A.S. Verhoeven, B. Demmig-Adams, W.W. Adams, Enhanced employment of the xanthophyll cycle and thermal energy dissipation in spinach exposed to high light and N stress, Plant Physiol. 113 (1997) 817–824, https://doi.org/10.1104/pp.113.3.817.

[70] B.A. Logan, B. Demmig-Adams, W.W. Adams, W. Bilger, Context, quantification, and measurement guide for non-photochemical quenching of chlorophyll fluorescence, (2014) 187–201. https://doi.org/10.1007/978-94-017-9032-1_7.

[71] B. Demmig-Adams, V. Ebbert, D.L. Mellman, K.E. Mueh, L. Schaffer, C. Funk, C. R. Zarter, I. Adamska, S. Jansson, W.W. Adams, Modulation of PsbS and flexible vs sustained energy dissipation by light environment in different species, Physiol. Plant. 127 (2006) 670–680, https://doi.org/10.1111/J.1399-3054.2006.00698.X.

[72] B. Demmig-Adams, W.W. Adams, Photoprotection in an ecological context: the remarkable complexity of thermal energy dissipation, New Phytol. 172 (2006) 11–21, https://doi.org/10.1111/J.1469-8137.2006.01835.X.

[73] J. Serôdio, J. Ezequiel, J. Frommlet, M. Laviale, J. Lavaud, A method for the rapid generation of Nonsequential light-response curves of chlorophyll fluorescence, Plant Physiol. 163 (2013) 1089–1102, https://doi.org/10.1104/PP.113.225243.

[74] A. Porcar-Castell, E. Tyystjärvi, J. Atherton, C. Van Der Tol, J. Flexas, E.E. Pfündel, J. Moreno, C. Frankenberg, J.A. Berry, Linking chlorophyll a fluorescence to

photosynthesis for remote sensing applications: mechanisms and challenges, J. Exp. Bot. 65 (2014) 4065–4095, https://doi.org/10.1093/jxb/eru191.

[75] H.M. Kalaji, G. Schansker, R.J. Ladle, V. Goltsev, K. Bosa, S.I. Allakhverdiev, M. Brestic, F. Bussotti, A. Calatayud, P. Dąbrowski, N.I. Elsheery, L. Ferroni, L. Guidi, S.W. Hogewoning, A. Jajoo, A.N. Misra, S.G. Nebauer, S. Pancaldi, C. Penella, D. Poli, M. Pollastrini, Z.B. Romanowska-Duda, B. Rutkowska, J. Serôdio, K. Suresh, W. Szulc, E. Tambussi, M. Yanniccari, M. Zivcak, Frequently asked questions about in vivo chlorophyll fluorescence: Practical issues, Photosynth. Res 122 (2014) 121–158, https://doi.org/10.1007/s11120-014-0024-6.

[76] L.N.M. Duysens, H.E. Sweers, Mechanism of two photochemical reactions in algae as studied by means of fluorescence, Stud. Microalgae Photosynth. Bact. (1963) 353–372, https://ci.nii.ac.jp/naid/10003748605 (accessed October 26, 2021).

[77] A. Stirbet, Govindjee, On the relation between the Kautsky effect (chlorophyll a fluorescence induction) and Photosystem II: Basics and applications of the OJIP fluorescence transient, J. Photochem. Photobiol. B Biol. 104 (2011) 236–257, https://doi.org/10.1016/j.jphotobiol.2010.12.010.

[78] G. Schansker, S.Z. Tóth, R.J. Strasser, Dark recovery of the Chl a fluorescence transient (OJIP) after light adaptation: The qT-component of non-photochemical quenching is related to an activated photosystem I acceptor side, Biochim. Biophys. Acta - Bioenerg. 1757 (2006) 787–797, https://doi.org/10.1016/j.bbabio.2006.04.019.

[79] R.J. Strasser, M. Tsimilli-Michael, S. Qiang, V. Goltsev, Simultaneous in vivo recording of prompt and delayed fluorescence and 820-nm reflection changes during drying and after rehydration of the resurrection plant Haberlea rhodopensis, Biochim. Biophys. Acta - Bioenerg. 1797 (2010) 1313–1326, https://doi.org/10.1016/J.BBABIO.2010.03.008.

[80] W.W. Adams, B. Demmig-Adams, Chlorophyll fluorescence as a tool to monitor plant response to the environment, (2004) 583–604. https://doi.org/10.1007/978-1-4020-3218-9_22.

[81] X. Yao, C. Li, S. Li, Q. Zhu, H. Zhang, H. Wang, C. Yu, S.K. St. Martin, F. Xie, Effect of shade on leaf photosynthetic capacity, light-intercepting, electron transfer and energy distribution of soybeans, Plant Growth Regul. 83 (2017) 409–416, https://doi.org/10.1007/S10725-017-0307-Y/TABLES/6.

[82] M. Zivcak, M. Brestic, H.M. Kalaji, Govindjee, Photosynthetic responses of sun- and shade-grown barley leaves to high light: Is the lower PSII connectivity in shade leaves associated with protection against excess of light? Photosynth. Res. 119 (2014) 339–354, https://doi.org/10.1007/s11120-014-9969-8.

[83] B. Ospina Calvo, T.L. Parapugna, M.G. Lagorio, Variability in chlorophyll fluorescence spectra of eggplant fruit grown under different light environments: A case study, Photochem. Photobiol. Sci. 16 (2017) 711–720, https://doi.org/10.1039/c6pp00475j.

[84] R.J. Strasser, M. Tsimilli-Michael, A. Srivastava, Analysis of the chlorophyll a fluorescence transient BT - chlorophyll a fluorescence: A Signature of Photosynthesis, in: G.C. Papageorgiou, Govindjee (Eds.), Springer Netherlands, Dordrecht, 2004: pp. 321–362. https://doi.org/10.1007/978-1-4020-3218-9_12.

[85] G. Sipka, M. Magyar, A. Mezzetti, P. Akhtar, Q. Zhu, Y. Xiao, G. Han, S. Santabarbara, J.R. Shen, P.H. Lambrev, G. Garab, Light-adapted charge-separated state of photosystem II: Structural and functional dynamics of the closed reaction center, Plant Cell 33 (2021) 1286–1302, https://doi.org/10.1093/plcell/koab008.